I&EC research
Industrial & Engineering Chemistry Research

pubs.acs.org/IECR
Article

Using an Innovative Concentric Cube Electrochemical Reactor for High-Efficiency H_2O_2 Production and Atrazine Degradation

Andre Luis Carvalho Souza, Raul José Alves Felisardo,* Robson da Silva Souto,* Renata Colombo, and Marcos Roberto de Vasconcelos Lanza*

Cite This: https://doi.org/10.1021/acs.iecr.6c00181
Read Online

ABSTRACT: This study reports the optimization of a continuous-flow electrochemical reactor with concentric cube geometry designed for the in-situ production of hydrogen peroxide (H_2O_2). The system, developed using a Printex L6 carbon-based gas diffusion electrode (GDE), was optimized and applied for high-efficiency H_2O_2 generation and the remediation of atrazine (ATZ) contaminated water. The initial analysis of different volumetric flow rates (200, 400, and 800 mL min^{-1}) showed that the rate of 400 mL min^{-1} offered the best balance between H_2O_2 production efficiency, energy consumption (7.57 kWh kg^{-1}), and current efficiency (78.1%). A central composite rotatable design (CCRD) was applied for the analysis of the effects of current density, electrolyte concentration, oxygen flow rate, and pH. The CCRD model exhibited high predictive accuracy ($R^2 > 0.96$), with current density and pH identified as the most influential factors. With a working volume of 1 L, under optimal conditions (0.075 mol L^{-1} K_2SO_4, 20 mA cm^{-2}, 0.05 L min^{-1} O_2, pH 5), 848 mg L^{-1} of H_2O_2 were generated in 30 min. Among the oxidative processes tested, the combined AO/e-H_2O_2/UVC treatment recorded >90% ATZ removal and >23% mineralization in 30 min, evidencing a strong synergistic effect attributed to UVC-induced H_2O_2 photolysis and hydroxyl radical formation. LC-MS/MS analysis confirmed the formation of 11 oxidative intermediates, where the degradation pathways were found to involve dechlorination, N-dealkylation, and cleavage of the s-triazine ring. The results of this study highlight the application potential of innovative reactor designs for efficient H_2O_2 electrogeneration and sustainable mitigation of persistent organic pollutants.

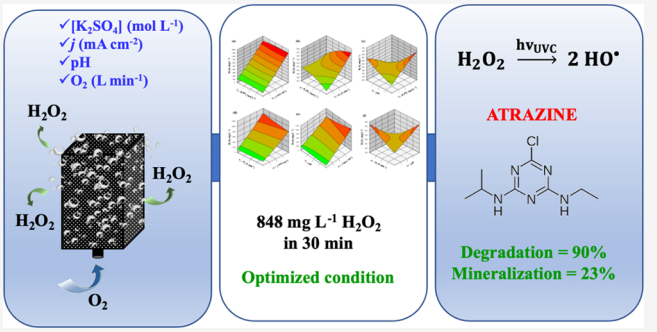

1. INTRODUCTION

The continuous growth of the global population requires a proportional increase in the production of food, pharmaceuticals, and other essential goods in order to sustain modern life. As expected, the massive increase in the production of these goods has inevitably resulted in the generation of increasingly larger quantities of organic waste. One clear example is agricultural production, which relies heavily on the intensive use of pesticides for pests control and the enhancement of productivity in crop production.[1−3] Over the past few decades, reports in the literature have shown that the advent and development of agrochemicals of different classes—including herbicides, insecticides, and fungicides, have resulted in the progressive intensification of their use in agricultural production for weeds and pests control and for boosting efficiency in crop yields.[4] Because of their persistent chemical nature, these agrochemical compounds exhibit a high potential for environmental transport, leading to the contamination of diverse water bodies, from surface water to groundwater systems.[5,6]

Among these agrochemical compounds, atrazine (ATZ, $C_8H_{14}ClN_5$), which is primarily applied in maize and sugar cane cultivation, stands out as one of the most widely used pesticides worldwide.[7,8] The major concern regarding the widespread use of atrazine lies in its recalcitrant character, high chemical stability, and environmental persistence; these factors clearly contribute to the frequent detection of the compound in aquatic systems even after they have been subjected to conventional treatment processes.[8,9] This issue extends beyond the mere occurrence of ATZ in aquatic environments, as prolonged exposure to ATZ has been associated with significant ecotoxicological risks and potential adverse effects on human health.[10]

In order to mitigate the negative impacts of these recalcitrant pollutants on human health and on the ecosystems, the scientific community has increasingly devoted substantial efforts to developing technologies that are capable of efficiently

Received: January 13, 2026
Revised: March 3, 2026
Accepted: March 6, 2026

https://doi.org/10.1021/acs.iecr.6c00181
Ind. Eng. Chem. Res. XXXX, XXX, XXX−XXX

removing them from wastewater and contaminated water worldwide. Considering that conventional wastewater treatments have often shown considerable limitations when they are used in degrading these recalcitrant compounds,[11−13] advanced oxidation processes (AOP), and particularly electrochemical advanced oxidation processes (EAOP), have emerged as promising alternatives. EAOP relies on the *in situ* generation of highly reactive species, such as hydroxyl radicals ($^{\bullet}OH$), which possess strong oxidizing power and remarkable ability to degrade persistent organic pollutants. These treatment processes provide a more efficient and sustainable approach for the treatment of contaminated water and wastewater.[14]

The use of hydrogen peroxide (H_2O_2) in water and wastewater treatment has proven to be a safe and efficient strategy for degrading recalcitrant compounds. With an oxidation potential of 1.76 V, H_2O_2 can be activated to generate $^{\bullet}OH$ (E = 2.80 V), which reacts nonselectively and is capable of decomposing persistent contaminants.[15] H_2O_2 can be produced through various methods, among which the anthraquinone oxidation process remains the most widely applied on an industrial scale.[16] However, when it comes to H_2O_2 production processes, the in-situ electrochemical generation mechanism has emerged as a highly efficient alternative process that is not only cost-effective but also considerably more sustainable, compared to other conventional techniques;[17,18] this in-situ electrochemical process mainly occurs via the two-electron oxygen reduction reaction ($2e^-$ ORR), as described in eq 1.[18,19]

$$O_2 + 2H^+ + 2e^- \rightarrow H_2O_2 \quad (1)$$

In order to obtain efficient results, the use of highly effective, selective, and low-cost electrodes in in-situ H_2O_2 electrogeneration processes is essentially important. Due to their abundance, favorable electrochemical properties, and high selectivity toward the two-electron oxygen reduction pathway, carbon-based materials are among the most promising candidates when it comes to the choice of materials for electrode construction;[18,20−22] these materials are suitable for designing gas diffusion electrodes (GDE) whose triple-phase configuration (gas/solid/liquid) optimizes O_2 transport and helps overcome limitations associated with the low solubility of oxygen in the liquid phase.[23−25]

Optimizing these carbon-based materials and construction of high-performance GDEs are directly linked to the performance and efficiency of electrochemical reactors; this is because successful H_2O_2 generation depends not only on the electrochemical properties of the electrode but also on its integration into properly designed reaction systems. The use of electrochemical reactors in water and wastewater treatment has become increasingly relevant due to their applicability under near-real conditions. Such reactors can adopt different configurations, including monopolar or bipolar setups, and operate in batch, continuous stirred tank, or continuous-flow modes.[26] Among the aforementioned operating modes, reactors operated under the continuous-flow mode have been found to be outstanding in the sense that they allow for easy integration with treatment plants and other remediation systems. Despite growing interest among researchers, few studies have explored the use of flow reactors coupled with GDEs for the electrogeneration of H_2O_2, and this points to the need for conducting more studies targeted at exploring this type of reactor.

Taking the above observations into account, the present study aimed to develop and optimize a continuous-flow electrochemical reactor with a concentric-cube geometry for the in-situ production of H_2O_2. The study focused not only on maximizing the efficiency of electrochemical H_2O_2 generation but also on evaluating its application in the remediation of water contaminated with the herbicide atrazine using carbon-based Printex L6 gas diffusion electrodes. Critical operating parameters, including volumetric flow rate, current density, electrolyte concentration, oxygen flow, and pH, were systematically investigated; this allowed for the definition of optimal conditions for efficient ATZ degradation while ensuring a balance between the system performance and energy consumption. At its core, this work brings useful contributions to the subject matter by exploring and presenting new strategies for the design of continuous-flow electrochemical reactors coupled with gas diffusion electrodes; in doing so, the study seeks to help broaden our knowledge and understanding of in-situ H_2O_2 generation processes and their application in advanced water remediation technologies.

2. EXPERIMENTAL SECTION

2.1. Chemicals and Materials

The materials used for the fabrication of GDE included amorphous carbon Printex L6 (Evonik), 60% (w/w) poly(tetrafluoroethylene) (PTFE) dispersion (Daklon 1, Sealflon), and PX30-PW03 carbon cloth (ZOLTEK). Potassium sulfate (K_2SO_4)—acquired from Vetec (purity of 99%−99.5%), was used as the supporting electrolyte. The solution pH was adjusted using H_2SO_4 (from Exodus Cientfica, 95%) or KOH (from Synth, 85%). Analytical-grade Atrazine standard used in the experiments was obtained from Sigma−Aldrich. Oxygen gas for the GDE supply was provided by MESSER Gases for Life. Ultrapure water with a resistivity of ≥18 MΩ cm, obtained from a Milli-Q system, was used for the preparation of all solutions.

2.2. Gas Diffusion Electrode (GDE), Concentric Cube Electrochemical Reactor, and Electrolytic System

The Printex L6 carbon GDE (GDE/PL6C) was fabricated following the standard procedure developed by our research group (Valim et al.,[27] with some modifications). Briefly, the PL6C catalytic mass was dispersed in water and subsequently combined with 30% PTFE solution in a 4:1 ratio. The mixture was mechanically stirred for 45 min, and the semidry catalytic mass was evenly spread over carbon cloth with an area of 80 cm^2. The assembly was then placed in a metal mold and subjected to a hot sintering process using a heated hydraulic press (Solab SL-11) at 290 °C, under a pressure of 0.5 tons, for 90 min. The mass of PL6C used to prepare the GDE was employed without chemical pretreatment and dried at 100 °C for 24 h. Prior to each experiment, the GDE/PL6C was activated by electrolysis for 15 min at 20 mA cm^{-2}, with an oxygen flow of 0.1 L min^{-1} in 0.05 mol L^{-1} K_2SO_4 (pH ∼6). After being used, the reactor and electrode were rinsed with deionized water and dried naturally. Previous studies from our group have shown that the GDE/PL6C maintains stable electrochemical performance and high-efficiency H_2O_2 production over multiple cycles, with minimal cell potential fluctuations during 81 h of continuous operation,[28] confirming its robustness and long-term reliability for H_2O_2 generation and contaminant degradation.

The PL6C material has already been characterized in detail in study conducted by our research group.[20] To reinforce reproducibility in the context of the present work, complementary morphology and wettability analyses were performed on the GDE/PL6C electrode, including field-emission scanning electron microscopy (FEG-SEM) and contact angle measurements. The FEG-SEM images were obtained using a JEOL JSM-7200F microscope, and the contact angle measurements were performed with an Ossila goniometer. The complete set of results is presented in the Supporting Information (Figure S1). The FEG-SEM micrographs (Figures S1a,c) show a

https://doi.org/10.1021/acs.iecr.6c00181
Ind. Eng. Chem. Res. XXXX, XXX, XXX−XXX

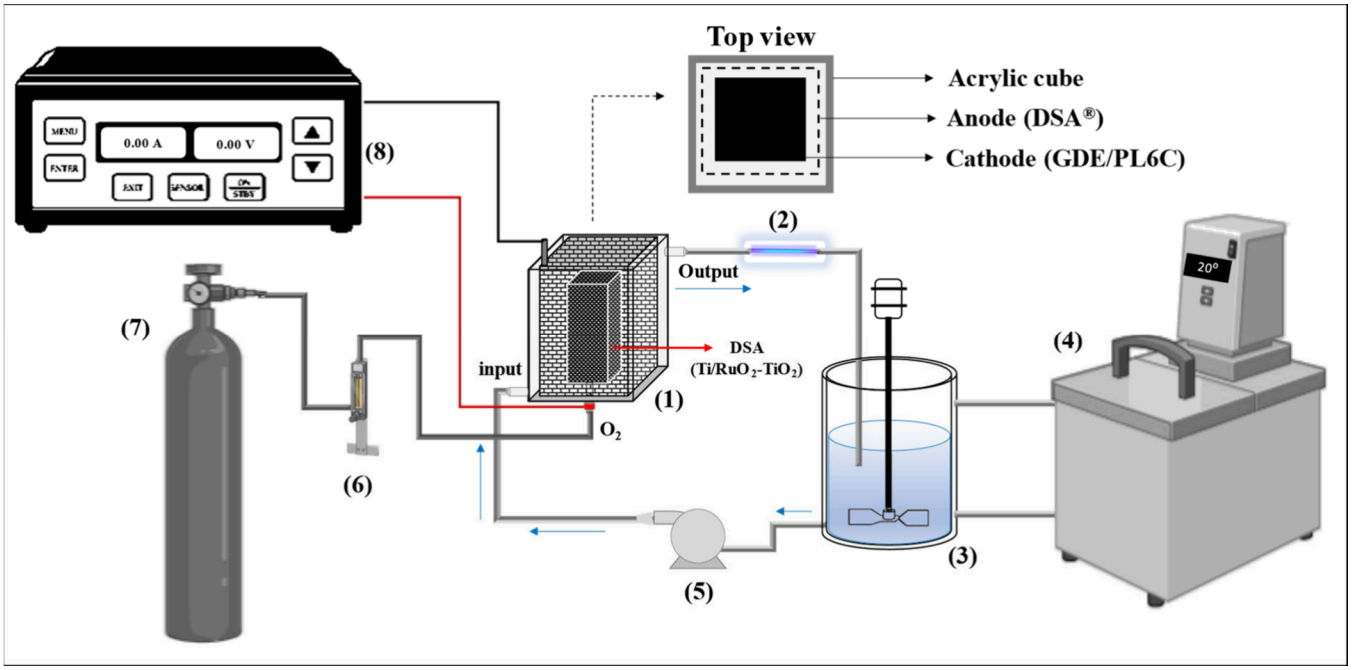

Figure 1. Schematic illustration of the experimental setup: (1) concentric-cube electrochemical reactor, (2) UVC light, (3) mixing tank, (4) thermostatic bath, (5) pump, (6) gas flow meter, (7) oxygen gas cylinder, and (8) current power supply.

homogeneous distribution of the PL6C layer on the carbon fabric, which acts as a structural support and current collector. The electrode surface exhibits a continuous and well-adhered coating, integrated into the fibrous substrate, without evidence of delamination or formation of compact agglomerates. Higher magnification images reveal a preserved porous and rough morphology, indicating effective integration between the catalytic phase and the conductive support. Contact angle analysis (Figure S1d) showed an average value of 106°, confirming the predominantly hydrophobic character of the surface.

The continuous-flow electrochemical reactor, designed with an internal concentric-cube geometry, is shown in Figure 1. The reactor was constructed by using six acrylic plates with internal dimensions of 45.5 cm^2. Three of these plates featured a central hole, two for hydrodynamic flow recirculation, and one for O_2 injection, as indicated. Concentric on this cube, an internal gas chamber was installed and used as the cathode; this system consisted of four active surfaces of the fabricated GDE/PL6C, totaling a geometric area of 96 cm^2, with continuous O_2 injection. The oxygen used was MESSER Gases and had a purity level of >99%.

In parallel, between the acrylic cube and the gas chamber, DSA-Cl_2 anodes (Ti/RuO_2−TiO_2), obtained from De Nora do Brazil, with a geometric area of 163 cm^2, were installed. This material was chosen due to its high electrochemical stability, operational durability, and catalytic efficiency, characteristics that promote greater system robustness and technological process predictions.[29,30] The working volume of the reactor was 192 mL. The concentric-cube electrochemical reactor was connected to a 1.0 L mixing tank, where the temperature was maintained at 20 °C by using a thermostatic bath (NOVA ÉTICA 521/2D). A magnetic stirrer (Fisatom 711), operating at 500 rpm, was used for mechanical stirring of the system. The system flow was driven by a hydraulic pump equipped with a flow meter (MS TECNOPON). Current was applied by using a Minipa DC power supply (MPS-3005B). For UVC light-assisted experiments, a 10 W Nuchong UVC lamp was installed between the reactor output and the mixing tank.

The concentric cube electrochemical reactor was selected to ensure a uniform current distribution between parallel planar electrodes and precise control of the interelectrode gap, thereby minimizing ohmic losses and enhancing energy efficiency. This configuration reduces edge effects and promotes a more homogeneous electric field, contributing to improved reproducibility of the electrochemical performance. Furthermore, the cubic design facilitates modular assembly and scalability, which are relevant for decentralized electrochemical treatment applications.

2.3. Determining the Operating Volumetric Flow Rate

A preliminary procedure was executed in order to evaluate the influence of volumetric flow (Q_v) rate on H_2O_2 generation, with a view to establishing a fixed rate for subsequent experiments. The tests were performed at a constant current density of 20 mA cm^{-2}, using an oxygen flow rate of 0.1 L min^{-1}, and a K_2SO_4 electrolyte concentration of 0.05 mol L^{-1} (natural pH = 6.00). The volumetric flow rate of the circulating solution was evaluated at the following varying rates: 200, 400, and 800 mL min^{-1}; this was done in order to investigate potential hydrodynamic effects, ranging from slower flows, which favor longer residence time and possible accumulation of H_2O_2, to higher flows, which may enhance mass transport and the removal of species formed at the electrode/solution interface.

2.4. Experimental Design and Statistical Validation

An experimental design was carried out in order to optimize the operational conditions of the system used for H_2O_2 electrogeneration; this allowed controlled variation of the studied parameters rather than maintaining them at fixed values. After the volumetric flow rate was selected from the preliminary tests, a central composite rotatable design (CCRD) was employed using a 2^4 factorial model with two coded levels, considering four independent variables: K_2SO_4 concentration (mol L^{-1}), current density (j, mA cm^{-2}), O_2 flow rate (L min^{-1}), and pH. The CCRD was chosen due to its ability to explore nonlinear relationships, identify optimal variable levels, and efficiently model both interaction and quadratic effects, as described by the mathematical model in eq 2.[31]

$$Y = b_0 + b_1x_1 + b_{11}x_1^2 + b_2x_2 + b_{22}x_2^2 + b_3x_3 + b_{33}x_3^2 + b_4x_4 + b_{44}x_4^2 + b_{12}x_2x_2 + b_{13}x_1x_3 + b_{14}x_1x_4 + b_{23}x_2x_3 + b_{24}x_2x_4 + b_{34}x_3x_4 + b_{123}x_1x_2x_3 + b_{124}x_1x_2x_4 + b_{134}x_1x_3x_4 + b_{234}x_2x_3x_4 + b_{1234}x_1x_2x_3x_4 \quad (2)$$

where Y represents the predicted response, while x_1, x_2, x_3, and x_4 correspond to the independent variables. The coefficient b_0 represents

https://doi.org/10.1021/acs.iecr.6c00181
Ind. Eng. Chem. Res. XXXX, XXX, XXX−XXX

the overall mean; b_1, b_2, b_3, and b_4 represent the linear effects; b_{11}, b_{22}, b_{33}, and b_{44} represent the quadratic effects; and b_{12}, b_{13}, b_{14}, b_{23}, b_{24}, and b_{34} represent the second-order interactions. The terms b_{123}, b_{124}, b_{134}, b_{234}, and b_{1234} represent the third- and fourth-order interactions, which allow a comprehensive analysis of variable combinations.

Table 1 presents the experimental matrix and combinations proposed by the CCRD. The levels of the independent variables

Table 1. CCRD Matrix for a 2^4 Factorial Design, Showing Coded Input Variables and Their Corresponding Actual Values for the Analysis of H_2O_2 Production in a Concentric-Cube Electrochemical Reactor

	Levels				
Factor	$-\alpha$ (−1.68)	−1	0	+1	$+\alpha$ (+1.68)
x_1: K_2SO_4 concentration in mol L^{-1}	0.008	0.025	0.050	0.075	0.092
x_2: Current density in mA cm^{-2}	6.59	10.00	15.00	20.00	23.41
x_3: O_2 flow in L min^{-1}	0.033	0.05	0.075	0.100	0.117
x_4: pH	3.63	5.00	7.00	9.00	10.36

were coded as +1 (high), −1 (low), 0 (central level), $+\alpha$, and $-\alpha$, based on the limits defined by the CCRD. The K_2SO_4 concentration (x_1) ranged from 0.025 mol L^{-1} (−1) to 0.075 mol L^{-1} (+1), with a central level of 0.05 mol L^{-1} (0). These values were chosen considering the influence of the sulfate ion concentration on solution conductivity and process efficiency. Lower concentrations may limit conductivity, while higher concentrations may lead to excessive electrolyte consumption.[32]

Current density (x_2) was adjusted between 5 mA cm^{-2} (−1) and 15 mA cm^{-2} (+1), with a central level of 10 mA cm^{-2} (0). This range was defined based on electrochemical conditions that balance H_2O_2 generation efficiency and system stability, avoiding undesired byproducts at high currents and waste of energy.[33] The applied O_2 flow rate (x_3) varied between 0.05 L min^{-1} (−1) and 0.1 L min^{-1} (+1), with a central level of 0.075 L min^{-1} (0); this variable ensured adequate reactant supply to overcome mass transfer limitations, thereby allowing the applied current to control the H_2O_2 generation rate. Simultaneously, the gas stream provides a counter-pressure to the liquid flow on the opposite side of the GDE, preventing electrode flooding and preserving stable gas−liquid interface conditions during operation.[34] The pH level (x_4) was adjusted between 5 (−1) and 9 (+1), with a central level of 7 (0); this range was chosen considering the impact of pH on electrode reactivity and H_2O_2 stability. Lower pH values favor proton availability, while higher pH values can accelerate H_2O_2 decomposition.[35] It should be noted that all pH values reported correspond to the initial pH values of the solutions. The amount of H_2O_2 generated after 30 min of electrolysis was used as the response variable in the CCRD.

The CCRD results were represented as response surfaces using Protimiza Experimental Design, and the mathematical-statistical regression model was validated through analysis of variance (ANOVA). Experiments were conducted in a randomized order to minimize uncontrolled variability, and six replicates at the central point allowed for the detection of curvature and the estimation of pure error. All assays were carried out at 20 °C, and the solution pH was adjusted using an Ion pHB500 pH meter.

2.5. Degradation of Atrazine

Under the optimized CCRD conditions for H_2O_2 electrogeneration (e-H_2O_2) and the volumetric flow (Q_z) rate selected from the preliminary tests, atrazine (ATZ) degradation assays were performed in order to evaluate the efficiency of the system in treating synthetic agro-industrial effluents. ATZ was used at a concentration of 10 mg L^{-1}. The experiments were performed in galvanostatic mode, and samples were collected at defined time intervals for subsequent analyses. In addition to the anodic oxidation process coupled with H_2O_2 electrogeneration (AO/e-H_2O_2), other AOPs were investigated; these included e-H_2O_2, AO, AO/e-H_2O_2/UVC, and UVC. For processes without in-situ H_2O_2 generation, N_2 was used at the volumetric flow rate optimized under the CCRD.

2.6. Analytical Procedures

H_2O_2 was quantified using the ammonium molybdate method,[36] determined on a Shimadzu Model V-1900 spectrophotometer. The current efficiency (CE) of H_2O_2 electrogeneration was expressed as a percentage and was determined by eq 3. The calculation of energy consumption (EC) in H_2O_2 electrogeneration, expressed in terms of kWh kg^{-1} of H_2O_2 produced, was performed using eq 4.

$$\mathrm{CE}\ (\%) = \frac{n \cdot F \cdot C \cdot V}{I \cdot t} \times 100 \tag{3}$$

$$\mathrm{EC}\left(\frac{\mathrm{kWh}}{\mathrm{kg}}\right) = 1000 \times \frac{I \cdot E \cdot t}{V \cdot C} \tag{4}$$

where n is the number of electrons involved in the reaction ($2e^-$), F the Faraday constant (96 487 C mol^{-1}), C the H_2O_2 concentration (mg L^{-1}), V the solution volume (L), I the applied electric current (A), and t the electrogeneration time (s) or (h).

The ATZ concentration was determined by high-performance liquid chromatography (HPLC-UVC, Shimadzu Model 20A HPLC). The analytical column employed was C18 with a particle size of 5 μm and dimensions of 4.6 mm × 150 mm; the equipment was maintained at a constant temperature of 30 °C. The mobile phase was composed of 70% acetonitrile and 30% water, eluted at a volumetric flow rate of 1 mL min^{-1}. The total run time applied was 6 min, and well-defined peaks were identified at λ = 222 nm in 4.7 min. The injection volume was 20 μL, and all samples were filtered using Chromafil Xtra PET-45/25 filters (pore size of 0.45 μm).

The percentage of ATZ degradation (%ATZ) was calculated based on eq 5, where c_0 is the initial concentration and c_t is the concentration at a given time t.

$$\%\mathrm{ATZ} = \frac{C_0 - C_t}{C_0} \times 100 \tag{5}$$

The energy consumed per volume of treated effluent (EC) was calculated using eq 6, where E_{cell} is the average cell potential (V), t the electrolysis time (h), V_s the volume of the solution (m^3), and I the current (A):

$$\mathrm{EC}\ (\mathrm{Wh\ m^{-3}}) = \frac{E_{cell} I t}{V_s} \tag{6}$$

Mineralization was determined through total organic carbon (TOC) using a Shimadzu TOC-L Series carbon analyzer. TOC removal was calculated based on eq 7, where TOC_0 is the initial value and TOC_t is the value at time t.

$$\mathrm{TOC\ removal}\ (\%) = \frac{\mathrm{TOC}_0 - \mathrm{TOC}}{\mathrm{TOC}_0} \times 100 \tag{7}$$

The energy consumed per unit mass of TOC removed (EC_{TOC}) was determined using eq 8, where E_{cell} is the average cell potential (V), t the electrolysis time (h), V_s the solution volume (m^3), I the current (A), and Δ(TOC) the reduced TOC content.

$$\mathrm{EC_{TOC}}\ (\mathrm{kWh(g\ TOC)^{-1}}) = \frac{E_{cell} I t}{V_s \Delta(\mathrm{TOC})} \tag{8}$$

It should be noted that, for UVC-assisted processes, in the calculation of EC (Whm^{-3}) and EC_{TOC}($kWh(gTOC)^{-1}$), the 10 W of power added to E_{cell} was taken into account.

2.7. Identification of ATZ Degradation Intermediates Using LC−MS/MS

The intermediates produced during the oxidative degradation of ATZ were identified using liquid chromatography coupled to tandem mass spectrometry (LC−MS/MS). The analyses were carried out using a

https://doi.org/10.1021/acs.iecr.6c00181
Ind. Eng. Chem. Res. XXXX, XXX, XXX−XXX

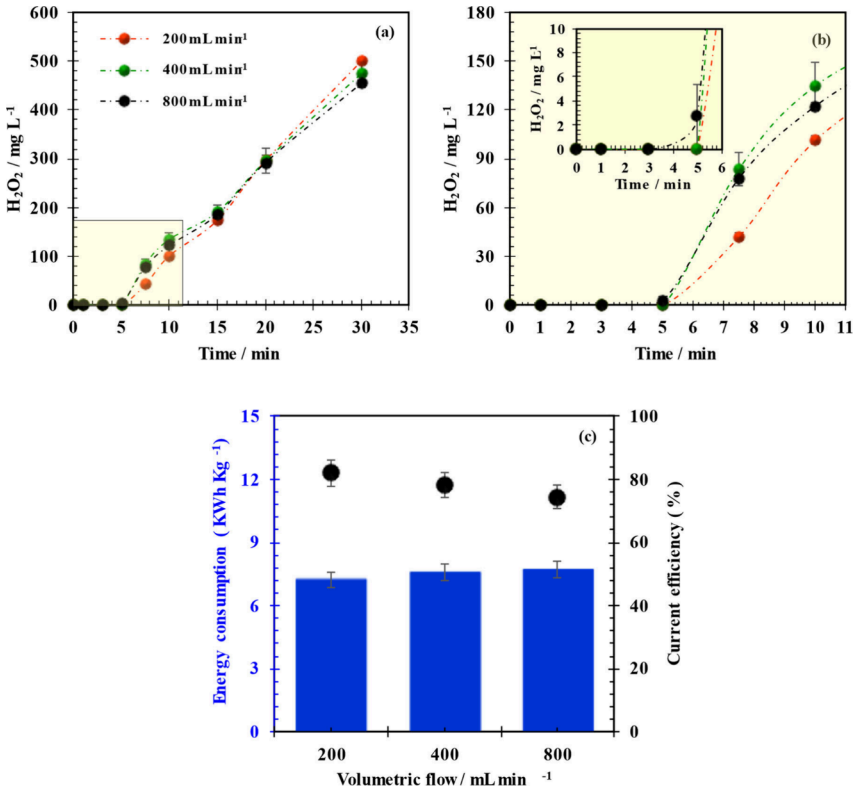

Figure 2. (a and b) Kinetic profiles of in-situ H_2O_2 generation recorded over 30 min of electrolysis in a concentric-cube electrochemical reactor for the flow rates of 200, 400, and 800 mL min^{-1}; (c) energy consumption and equivalent energy efficiency. Conditions applied: current density (j) = 20 mA cm^{-2}, O_2 = 0.1 L min^{-1}, K_2SO_4 = 0.025 mol L^{-1}, pH 6.00, and temperature (T) = 20 °C.

Shimadzu LC/MS-8030 triple quadrupole instrument (Japan). Separation was performed on a Shim-pack ODS II column (100 × 3.0 mm inner diameter, 2.2 μm particle size), kept at 30 °C. The mobile phase was composed of water (solvent A) and acetonitrile (solvent B), both containing 0.1% formic acid. The chromatographic run was conducted at a flow rate of 0.5 mL min^{-1} with the following gradient: 0−5 min, 10%−37% B; 5−8 min, 37%−100% B; 8−10 min, 100%−10% B. Mass spectrometric detection was performed using an electrospray ionization (ESI) source in positive-ion mode, operating at 400 °C and at the potential of 4.5 kV. Spectra were acquired in full-scan mode within the m/z range of 100−500. Nitrogen was applied as both the nebulizing and drying gas at flow rates of 3 and 15 L min^{-1}, respectively.

3. RESULTS AND DISCUSSION

3.1. Preliminary Assessment: Determining the Operating Volumetric Flow

As mentioned previously, different recirculation volumetric flow rates in the H_2O_2 electrogeneration (200, 400, and 800 mL min^{-1}) were analyzed in order to establish a fixed optimal rate for the subsequent optimization steps. In this analysis, the current density was set at 20 mA cm^{-2}, the oxygen flow was set at 0.1 L min^{-1}, the K_2SO_4 concentration was set at 0.05 mol L^{-1}, and the electrolyte was set at its natural pH (6.00). Figure 2 shows the H_2O_2 generation kinetics over 30 min of electrolysis, the equivalent energy consumption, and the energy efficiency of the respective volumetric flow rates. The kinetic profiles (Figure 2a) indicate similar behavior for flow rates of 200, 400, and 800 mL min^{-1}, with slight differences in the final accumulated H_2O_2 concentrations, which were 500, 475, and 453 mg L^{-1}, respectively. Although the flow rate quadrupled between the extreme conditions, the variation in the H_2O_2 concentration was less than 10%, evidencing that the process is not very sensitive to changes in the hydrodynamic range investigated in this study. These minor variations observed in the final H_2O_2 concentrations can also be attributed to increased contact between the circulating solution and the anode surface, where partial oxidation or decomposition of H_2O_2 may occur. Under high recirculation conditions, this effect becomes more pronounced due to the higher frequency of solution passage through the anode compartment, which explains the slight decrease in accumulation observed, despite adequate mass transfer.

The enlarged detailed illustration in Figure 2b points to the similarity between the curves; it essentially shows that the main difference lies in the time of the onset of H_2O_2 accumulation. The enlargement of the scale in Figure 2b points to the similarity between the curves; it shows that the onset of H_2O_2 generation and/or accumulation occurs only after approximately 5 min of electrolysis. This initial delay may be associated with the stabilization stage of the hydrodynamic regime in a closed recirculation system. Furthermore, it is possible that in the first few minutes, some of the H_2O_2 produced is rapidly consumed by parallel reactions (such as catalytic decomposition on the electrode surface), which delays its detection in solution.[37]

Although the magnitude of the variation is modest, a tendency toward greater H_2O_2 generation or accumulation is observed at lower flow rates. This behavior can be associated with the residence time (τ), which was approximately 0.96, 0.48, and 0.24 min for flow rates of 200, 400, and 800 mL min^{-1}, respectively. At lower flow rates, prolonged contact between the solution and electrode increases the probability of O_2 reduction, favoring the formation of H_2O_2.[38] On the other

https://doi.org/10.1021/acs.iecr.6c00181
Ind. Eng. Chem. Res. XXXX, XXX, XXX−XXX

Table 2. CCRD Matrix for Factorial 2^4 with Coded Input Variables and Real Values for the Analysis of H_2O_2 Production in 30 min of Electrolysis in the Concentric-Cube Electrochemical Reactor

Experiment number	x_1 [K_2SO_4] (mol L^{-1})	x_2 j (mA cm^{-2})	x_3 O_2 (L min^{-1})	x_4 pH	[H_2O_2] mg L^{-1} Experimental
1	(−1) 0.025	(−1) 10	(−1) 0.050	(−1) 5.00	310.4
2	(+1) 0.075	(−1) 10	(−1) 0.050	(−1) 5.00	318.5
3	(−1) 0.025	(+1) 20	(−1) 0.050	(−1) 5.00	667.3
4	(+1) 0.075	(+1) 20	(−1) 0.050	(−1) 5.00	848.8
5	(−1) 0.025	(−1) 10	(+1) 0.100	(−1) 5.00	252.2
6	(+1) 0.075	(−1) 10	(+1) 0.100	(−1) 5.00	306.8
7	(−1) 0.025	(+1) 20	(+1) 0.100	(−1) 5.00	680.4
8	(+1) 0.075	(+1) 20	(+1) 0,100	(−1) 5.00	730.0
9	(−1) 0.025	(−1) 10	(−1) 0.050	(+1) 9.00	269.2
10	(+1) 0.075	(−1) 10	(−1) 0.050	(+1) 9.00	177.7
11	(−1) 0.025	(+1) 20	(−1) 0.050	(+1) 9.00	606.5
12	(+1) 0.075	(+1) 20	(−1) 0.050	(+1) 9.00	413.5
13	(−1) 0.025	(−1) 10	(+1) 0.100	(+1) 9.00	336.3
14	(+1) 0.075	(−1) 10	(+1) 0.100	(+1) 9.00	332.3
15	(−1) 0.025	(+1) 20	(+1) 0.100	(+1) 9.00	772.1
16	(+1) 0.075	(+1) 20	(+1) 0.100	(+1) 9.00	744.8
17	(−1.68) 0.008	(0) 15	(0) 0.075	(0) 7.00	448.7
18	(+1.68) 0.092	(0) 15	(0) 0.075	(0) 7.00	498.7
19	(0) 0.050	(−1.68) 6.59	(0) 0.075	(0) 7.00	142.3
20	(0) 0.050	(+1.68) 23.41	(0) 0.075	(0) 7.00	882.6
21	(0) 0.050	(0) 15	(−1.68) 0.033	(0) 7.00	505.9
22	(0) 0.050	(0) 15	(+1.68) 0.117	(0) 7.00	501.4
23	(0) 0.050	(0) 15	(0) 0.075	(−1.68) 3.63	533.9
24	(0) 0.050	(0) 15	(0) 0.075	(+1.68) 10.36	486.8
25	(0) 0.050	(0) 15	(0) 0.075	(0) 7.00	490.0
26	(0) 0.050	(0) 15	(0) 0.075	(0) 7.00	505.2
27	(0) 0.050	(0) 15	(0) 0.075	(0) 7.00	479.3
28	(0) 0.050	(0) 15	(0) 0.075	(0) 7.00	480.8
29	(0) 0.050	(0) 15	(0) 0.075	(0) 7.00	481.3
30	(0) 0.050	(0) 15	(0) 0.075	(0) 7.00	447.1

hand, under high recirculation conditions, the reduced residence time can limit effective charge transfer at the electrode/solution interface,[38] in addition to intensifying O_2 carryover and dispersion, which contribute to the slight decrease in H_2O_2 accumulation. This effect is typical of closed-loop systems in which the flow rate simultaneously regulates reactor homogenization, dissolved oxygen supply, and the solution−catalyst contact rate.

The data on energy consumption in Figure 2c corroborate this analysis. Specifically, energy consumption increased slightly with the flow rate, from 7.26 kWh kg^{-1} at 200 mL min^{-1} to 7.70 kWh kg^{-1} at 800 mL min^{-1}, while current efficiency showed an inverse trend, decreasing from 82.1% to 74.5%. This suggests that, at higher flow rates, some of the applied electrical energy is not effectively converted to H_2O_2, possibly due to the shorter solution residence time in the reactor and the intensification of side reactions or H_2O_2 decomposition in the medium.

Thus, although the 200 mL min^{-1} flow rate condition exhibited a slight advantage in terms of the final H_2O_2 concentration and current efficiency, the flow rate of 400 mL min^{-1} represents the best operating compromise/balance. The 400 mL min^{-1} flow rate condition combines a final H_2O_2 concentration close to the maximum obtained, intermediate energy consumption (7.57 kWh kg^{-1}), and satisfactory current efficiency (78.1%), in addition to favoring a stable and reproducible hydrodynamic regime for subsequent tests. Furthermore, considering that the reactor will be used for ATZ degradation, moderate recirculation can ensure adequate renewal of the solution over the electrode, ensuring a continuous supply and a better distribution of H_2O_2 in the reaction volume.

The results showed that, within the evaluated hydrodynamic range, the variation in H_2O_2 production remains modest, indicating that the system operates under conditions where mass transfer is not the dominant limiting factor. This balance suggests that the reactor design ensures efficient gas−liquid−electrode interaction across a broad range of flow conditions, providing operational robustness and low sensitivity of H_2O_2 generation to hydrodynamic fluctuations.

3.2. Applying CCRD for the Optimization of H_2O_2 Electrogeneration in a Concentric-Cube Electrochemical Reactor

A thorough analysis of the in-situ generation of H_2O_2 under different operating conditions is essentially important, because it helps one to understand the factors that influence the system efficiency and to optimize the parameters of the process. Considering the operating system volumetric flow rate of 400 mL min^{-1}, as previously discussed, the CCRD, under the outlined conditions, for the supporting electrolyte concentration, current density, O_2 flow, and pH, was performed in 30 experiments using different combinations, as shown in eq 9.

$$\text{number of experiments} = r(2^k + 2k) + cp \quad (9)$$

https://doi.org/10.1021/acs.iecr.6c00181
Ind. Eng. Chem. Res. XXXX, XXX, XXX−XXX

where r is the number of genuine replicates (1), k is the number of independent variables (4), and cp is the number of replicates at the central point (6).

Table 2 presents the resulting CCRD matrix for analyzing H_2O_2 production over 30 min of electrolysis in the proposed concentric-cube electrochemical reactor. It is worth noting that the amount of H_2O_2 produced in the cp experiments (experiments 25−30) ranged from 447.1 mg L^{-1} to 505.2 mg L^{-1}. These results indicate variability in H_2O_2 production even under the same experimental conditions, which may be associated with small operational fluctuations such as variations in oxygen distribution. However, given the rotational complexity of the CCRD, this 58.1 mg L^{-1} fluctuation can be considered insignificant, considering the magnitude of the CCRD. Furthermore, the low data dispersion across the 5 cP replicates reinforces the reliability of the results, demonstrating that the system presents good reproducibility within the expected range for this type of experimental design.

The relative fluctuations observed in H_2O_2 production at the central point further indicate that localized hydrodynamic effects within the cubic reactor geometry have a minimal impact on the overall performance. While corner regions may theoretically experience slightly reduced convective flow, potentially leading to thicker diffusion layers and minor mass transport limitations, the upward recirculation flow, combined with the strategic placement of the inlet at the bottom and the outlet at the top, ensures continuous electrolyte renewal and effective mixing throughout the reactor.

A further point worth considering is that, in experiment number 20, H_2O_2 production and/or accumulation reached the maximum amount in the design, equivalent to 882.6 mg L^{-1}. As highlighted, this concentration was reached when the system was operating under the following conditions: K_2SO_4 = 0.05 mol L^{-1}, j = 23.41 mA cm^{-2}, O_2 = 0.05 L min^{-1}, and pH 7.00. It can be observed that the applied current density was at its maximum value at the axial point ($+\alpha$), while the other variables were within the ±1 limit. This behavior indicates that, although the current density exerted a decisive role in maximizing H_2O_2 production when adjusted in the axial range, possibly due to the increased electron transfer rate for the oxygen reduction reaction on the electrode surface, maintaining the other variables at moderate levels may have helped prevent the occurrence of adverse effects. This effect was also observed in experiment 4, which yielded the second-highest H_2O_2 production rate. In this case, all the variables evaluated were within the limit of ±1 (K_2SO_4 = 0.075 mol L^{-1}, j = 20 mA cm^{-2}, O_2 = 0.05 L min^{-1} and pH 5.00); in essence, this shows that the complexity of CCRD goes far beyond linear interactions, and process optimization should not only consider the individual maximum values of the variables but also their interactions and quadratic effects.

These adverse effects of interactions between variables can be analyzed using the mathematical regression model generated by the CCRD presented in eq 10.

$$[H_2O_2] = 480.62 + 3.25x_1 - 4.16x_1^2 + 193.37x_2 + 5.53x_2^2 + 22.24x_3 + 3.32x_3^2 - 23.18x_4 + 4.99x_4^2 + + 14.97x_2x_3 - 19.842.72x_1x_2 + 10.49x_1x_3 - 38.12x_1x_4x_2x_4 + 55.88x_3x_4 \quad (10)$$

This model describes the H_2O_2 concentration response as a function of the linear, quadratic, and interaction effects of variables x_1, x_2, x_3, and x_4. The constant term 480.62 represents the mean value of the H_2O_2 concentration when all variables are at the cp of the CCRD (Table 2, experiments 25−30), while analysis of the coefficients associated with the variables reveals the relative importance of each factor.

The results showed that the x_2 variable (current density) stands out as one of the most influential parameters, with a high linear coefficient of 193.37, which points to its strong positive effect on H_2O_2 concentration. The quadratic coefficient of x_2, equivalent to 5.53, also positive, indicates a parabolic effect and tends to increase as the current density increases, reinforcing the intensity of this positive effect. On the other hand, the x_4 variable (pH) has a considerable negative effect in the linear term (−23.18), indicating that increases in pH tend to reduce the H_2O_2 concentration. Furthermore, the quadratic coefficient of x_4 is positive, suggesting that, at high levels, pH actually has a less-pronounced effect on the H_2O_2 concentration. Regarding the x_1 variable (K_2SO_4 concentration), a moderately positive linear coefficient of 3.25 shows a milder positive impact on H_2O_2 concentration, which essentially indicates a slight increase in the response as K_2SO_4 concentration increases; however, the negative quadratic coefficient of this variable suggests that, at high K_2SO_4 concentration levels, when analyzed in isolation, the H_2O_2 concentration may begin to decrease. This nonlinear behavior suggests that x_1 has an ideal point beyond which its initial positive effect begins to diminish. A careful analysis of the effects of interactions showed that the interactions between x_1x_2 and x_2x_3 presented positive coefficients of 2.72 and 14.97, respectively. These positive interactions indicate a moderate increase in H_2O_2 concentration when the K_2SO_4 concentration, current density, and O_2 flow interact at their high levels. On the other hand, the interaction between x_2x_4, with a negative coefficient of −19.84, demonstrates that the combined increase in current density and pH can reduce the concentration of H_2O_2 generated.

A comprehensive analysis of the results obtained using the mathematical-statistical regression model reinforces that the complexity of the CCRD extends far beyond simply evaluating the main effects of the independent variables. It is observed that, in certain cases, the isolated or even quadratic effects of the variables exhibit antagonistic behaviors in relation to the H_2O_2 generation response, especially when compared to the effects of interactions between variables. In this context, response surface methodology (RSM) analysis becomes essential for a more-accurate interpretation of the results; this is because it allows for the identification of synergies and antagonisms between the experimental factors. This approach is crucial for determining the optimal operating conditions that maximize the efficiency of the reactor, in terms of H_2O_2 electrogeneration.

https://doi.org/10.1021/acs.iecr.6c00181
Ind. Eng. Chem. Res. XXXX, XXX, XXX−XXX

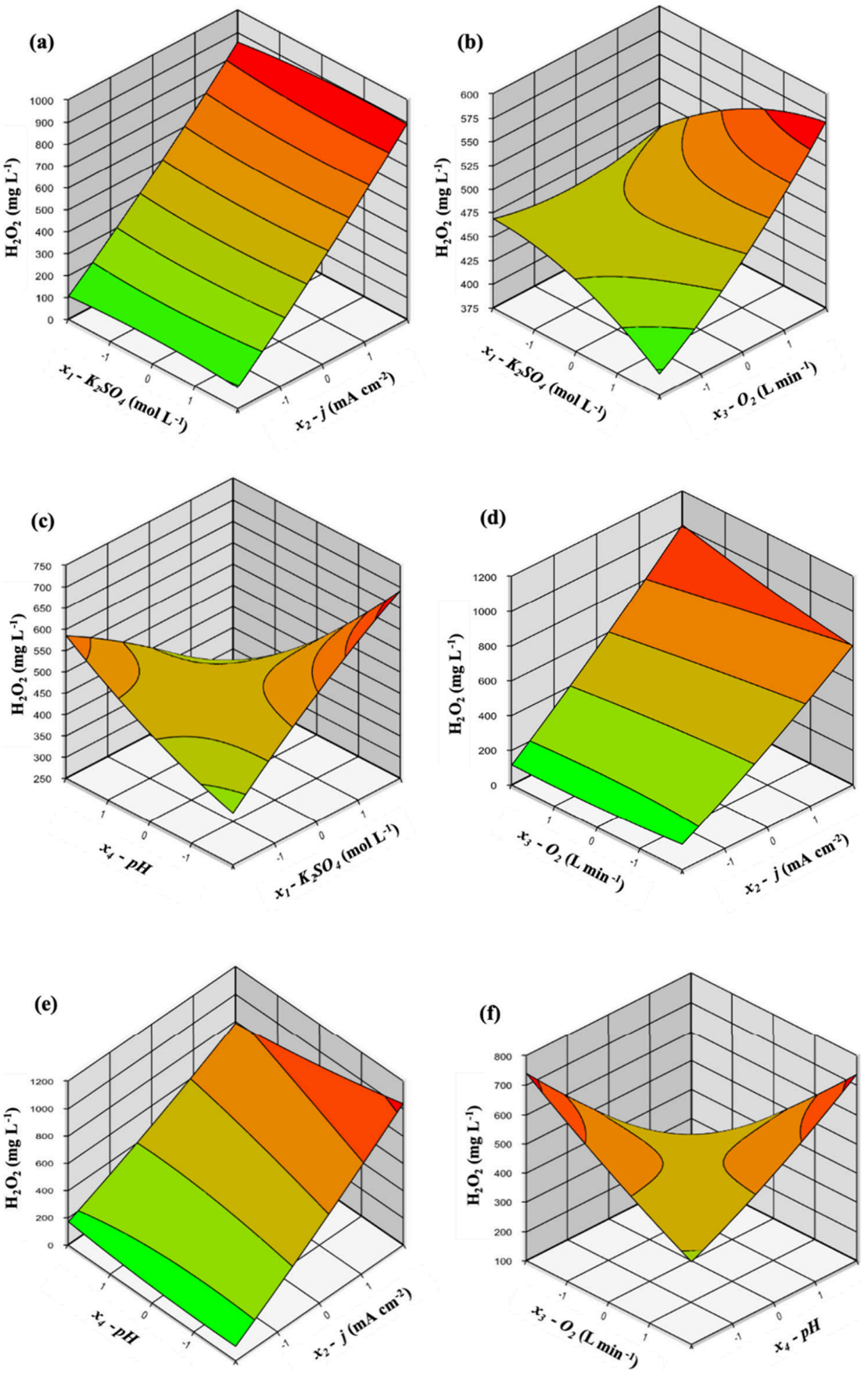

Figure 3. Response surface plots of the interactions established in the CCRD between (a) K_2SO_4 concentration vs current density, (b) K_2SO_4 concentration vs O_2 flow, (c) K_2SO_4 concentration vs pH, (d) current density vs O_2 flow (e) current density vs pH, and (f) O_2 flow vs pH as a function of H_2O_2 electrogeneration in 30 min of electrolysis in the concentric-cube electrochemical reactor.

https://doi.org/10.1021/acs.iecr.6c00181
Ind. Eng. Chem. Res. XXXX, XXX, XXX−XXX

3.3. RSM Analysis of the Interactions between the Input Variables

Figure 3 shows the RSM analysis conducted for CCRD in this work. It should be noted that, in these representations, the red region represents the critical region where H_2O_2 production reaches its maximum, while the green area represents the regions where H_2O_2 production becomes limited or inefficient. Figure 3a shows the interaction between the K_2SO_4 concentration and current density. It can be observed that, across the entire concentration range evaluated, an increase in K_2SO_4 concentration did not result in significant variations in H_2O_2 production. On the other hand, an increase in current density had a clear positive effect, with values above the central point ($j \geq 15$ mA cm^{-2}) exhibiting more significant effects. This behavior indicates that, in this interaction, although electrolyte concentration is important to ensure minimum conductivity of the medium, its variation within the tested limits does not significantly influence the efficiency of the process. In contrast, current density can act directly on the electrochemical reaction rate, increasing the flow of electrons available for the reduction of oxygen and, consequently, favoring the generation of H_2O_2.[38,39]

Interestingly, Figure 3b shows that the increase in K_2SO_4 concentration was highly significant when analyzed in interaction with the O_2 flow in GDE/PL6C. In this relationship, H_2O_2 production is maximized with the increase in both variables, and the effect of K_2SO_4 concentration is consistent throughout the studied range. In turn, O_2 flow values below the limit coded as −1 ($O_2 < 0.05$ L min^{-1}) do not favor H_2O_2 formation. H_2O_2 production reaches its maximum level when both K_2SO_4 concentration and O_2 flow are at levels above the point coded as +1 ($K_2SO_4 \geq 0.075$ mol L^{-1} and $O_2 \geq 0.1$ L min^{-1}). This behavior can be attributed to the fact that an increase in the concentration of the supporting electrolyte can contribute to reducing the ohmic resistance of the solution, promoting greater charge transfer efficiency and, consequently, favoring the electrochemical reactions of interest.[40] When associated with increased O_2 flow, this effect is enhanced, since the greater availability of molecular oxygen at the interface of the GDE/PL6C porous electrode ensures a higher reduction rate via two-electron transfer, the main pathway responsible for H_2O_2 generation.[41] Thus, this synergy between increased conductivity and greater availability of the gaseous reagent contributes significantly to the intensification of the reaction process.

K_2SO_4 concentration and pH showed a significant interaction effect on H_2O_2 production, as illustrated in Figure 3c. The response surface indicates that both variables influence the system synergistically, although excessive levels of both factors result in decreased H_2O_2 generation. At low supporting electrolyte concentrations ($K_2SO_4 < -1$, coded values), H_2O_2 production was enhanced under alkaline conditions (pH ≥1, corresponding to pH ≥ 9.0). In contrast, when the K_2SO_4 concentration exceeded the central level (≥0.05 mol L^{-1}), more-acidic conditions significantly favored H_2O_2 generation. The highest response region was observed between coded pH values from 0 to $-\alpha$ and K_2SO_4 concentrations from 0 to $+\alpha$. This behavior can be explained by the combined influence of the ionic conductivity, reaction kinetics, and oxidant stability. Increasing K_2SO_4 concentration enhances solution conductivity, facilitating charge transport and reducing ohmic losses within the electrochemical reactor. Under moderately acidic conditions, improved ionic mobility together with favorable proton availability promote the two-electron oxygen reduction reaction (ORR) pathway at the GDE surface, enhancing H_2O_2 electrogeneration. Additionally, acidic media increase H_2O2 stability by suppressing its catalyzed decomposition, thereby contributing to higher accumulation in solution.[42]

Figure 3d shows the relationship between the current density and the O_2 flow. In this interaction, the combination of a high current density and a high O_2 flow favors H_2O_2 generation. It can be observed that, throughout the entire extension range, an increase in current density resulted in an increase in H_2O_2 production, while the influence of O_2 flow is only significant at values above cp ($O_2 > 0.075$ L min^{-1}). It is likely that when the current density is high, the demand for oxygen at the electrode−solution interface increases as more electrons are being transferred and oxygen is needed to consume them. Under conditions of high O_2 flow, this demand is adequately met, enabling the reduction reaction to proceed more efficiently and with greater selectivity toward H_2O_2 production.[38,43] The positive influence exerted by an increase in the current density on H_2O_2 production is also observed in the interactions involving this variable and pH (Figure 3e). In this RSM, pH exerts a significant influence on H_2O_2 production only at coded values below −1 and in interactions involving high current density values, especially above the midpoint values. These results suggest that a high current density tends to be more effective in an acidic environment as it moderates side reactions that could compete with H_2O_2 formation. On the other hand, at very alkaline pH levels, H_2O_2 decomposition occurs faster, reducing the efficiency of H_2O_2 electrogeneration. This occurs because, in an alkaline environment, hydrogen peroxide is less stable and more prone to reaction, which compromises the process efficiency.[35]

Finally, Figure 3f shows the RSM of the interaction between the O_2 flow and pH. The dynamics between these variables demonstrate a nonlinear behavior, in which H_2O_2 production is favored both under conditions of high O_2 flux combined with alkaline pH and under conditions of low O_2 flow associated with acidic pH. An increase in H_2O_2 generation is observed when both variables are either at high levels ($O_2 \geq 0.1$ L min^{-1} and pH ≥9) or at low levels ($O_2 \leq 0.05$ L min^{-1} and pH ≤5). This complex behavior may be related to different dominant mechanisms under different operating conditions. In alkaline media, an increase in O_2 flow can enhance gas diffusion to the electrode interface, which maximizes the ORR rate via the two-electron pathway. In acidic media, even under lower O_2 flow conditions, the greater availability of protons (H^+) can favor the selectivity of ORR for the formation of H_2O_2 and increase the efficiency of the process, especially in GDE/PL6C.

Thus, the presence of different operational domains highlights the complexity and versatility of the system evaluated by using CCRD; this allows its optimization according to the specific conditions of the desired application. From this perspective, when one considers the best balance between H_2O_2 generation efficiency and nonextreme operating parameters, the condition of experiment number 4 (0.075 mol L^{-1} of K_2SO_4, current density of 20 mA cm^{-2}, O_2 flow of 0.05 L min^{-1}, and pH 5) stands out as one of the most promising, recording an output of 848.8 mg L^{-1} H_2O_2 (see Table 2). This configuration represents a technical, economic balance point that ensures high electrochemical performance without requiring intense operational conditions; this essentially makes experiment number 4 conditions highly viable for

https://doi.org/10.1021/acs.iecr.6c00181
Ind. Eng. Chem. Res. XXXX, XXX, XXX−XXX

conducting further ATZ degradation experiments in the GDE/PL6C-based concentric cube reactor.

3.4. Validating the Mathematical Statistical Regression Model in the Electrogeneration of H_2O_2 in the Concentric Cube Electrochemical Reactor

The response surface model described in eq 10 was validated using an analysis of variance (ANOVA) and Fisher's distribution (F-test). Table 3 presents the main statistical indicators relevant for this validation analysis. The significance of the model was assessed by comparing the observed and predicted values using the ratio of the mean square of the regression to the residual. In this sense, considering the degrees of freedom at a 90% confidence level, it is observed that the calculated value of $F_{Regression/residual}$, equivalent to 29.8, was higher than the tabulated F (1.985).

Table 3. Analysis of Variance (ANOVA) of the Experimental Results for H_2O_2 Electrogeneration in 30 min of Electrolysis Conducted Using a Concentric-Cube Electrochemical Reactor.(Conditions: T = 20 °C; Q_v = 400 mL min^{-1})

Variation source	Sum of squares	Degrees of freedom	Mean square	F_{calc}	p-value[a]
Regression	1009735.2	14	72123.9	29.8	0.00000
Residuals	36254.9	15	2417.0		
Lack of fit	34436.6	10	3443.7	9.5	0.01143
Pure error	1818.3	5	363.7		
Total	1045990.1	29			

[a] p-value regression <0.000001.

The model's goodness-of-fit was analyzed by comparing the mean square of the lack of fit with the pure error. In this analysis, the calculated value obtained was 9.5, which was above the theoretical tabulated value (3.29). This outcome suggests that, although the pure error is lower compared to the regression, the lack of fit is not negligible and exerts an influence on the model that was not considered in the design employed. Despite this observation, the ANOVA demonstrates that the regression model is statistically significant and adequately represents the experimental results with a p-value <0.001, considering that a model is deemed significant if at least one of its terms presents a significant correlation with the responses.[44] Furthermore, the mathematical model exhibits statistical predictability, with the $F_{Regression/residual}$ ratio >5;[45,46] this essentially shows that the model is able to explain approximately 96.53% of the total variance of the data, which reinforces its suitability for use in the optimization of H_2O_2 production in the concentric-cube electrochemical reactor, as it ensures a good correlation between the experimental values and the predicted values. The R^2 value suggests that the equation terms (linear, quadratic, and interaction) were appropriately selected to represent the studied phenomenon, and the model is highly effective in capturing the patterns of the observed data, with only 3.47% of the variation attributed to unmodeled factors, experimental uncertainties, or random disturbances.[47]

Data analysis and representation were also verified using a Pareto chart and by fitting the predicted and experimental values. In the Pareto chart (Figure 4a), the most significant variables and interactions for the model are those that exceed the critical t_{calc} value of ~2, which is represented by the red vertical line at the 10% significance level. The results are clearly in agreement with the behavior observed in the mathematical model; that is, among the variables studied, x_2 (current density) exhibits the strongest effect, and only x_1 (K_2SO_4 concentration) has no significant isolated effect. Figure 4b shows a good correlation between the predicted and experimental values, with points close to the diagonal line of identity; this implies that the model has enough predictive ability for the H_2O_2 generation response in the concentric-cube electrochemical reactor.

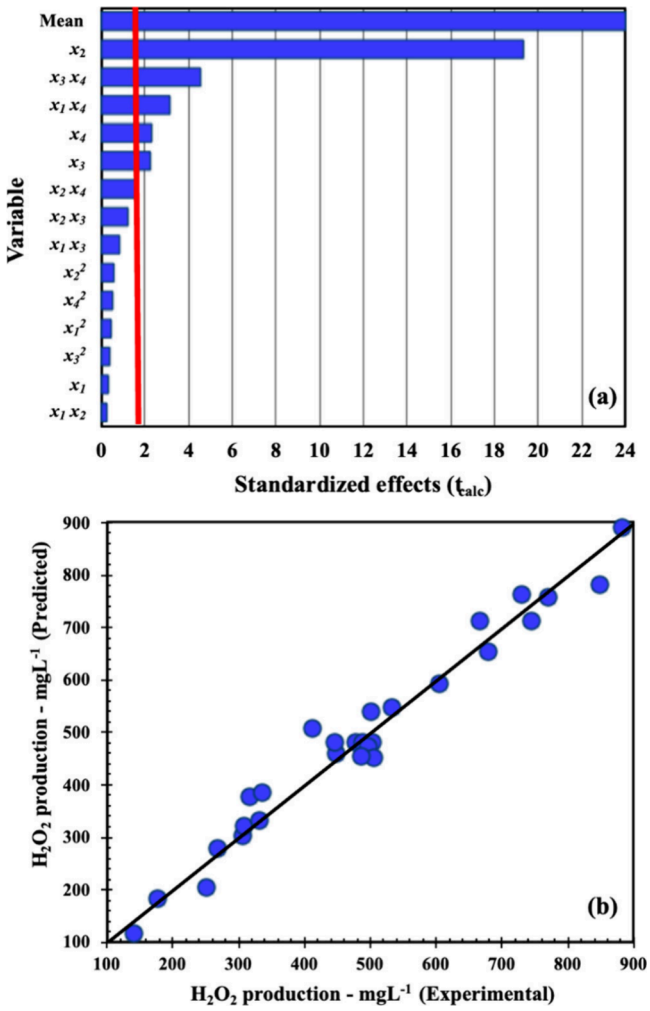

Figure 4. (a) Pareto chart and (b) predicted vs observed H_2O_2 electrogeneration values in the concentric-cube electrochemical reactor (conditions: T = 20 °C, Qv = 400 mL min^{-1}, and time (t) = 30 min).

3.5. Degradation and Mineralization of Atrazine under Optimized Conditions in a Concentric-Cube Electrochemical Reactor

Given the efficiency of the optimized condition obtained in the CCRD for the generation of H_2O_2 in the concentric-cube electrochemical reactor (x_1 – K_2SO_4 = 0.075 mol L^{-1}, x_2 – j = 20 mA cm^{-2}, x_3 – O_2 flow of 0.05 L min^{-1}, and x_4 – pH = 5.0), a thorough study was conducted targeted at the degradation of water contaminated with ATZ (C_0 = 10 mg L^{-1}) using different AOPs. The combined processes of anodic oxidation with electrogenerated hydrogen peroxide (AO/e-H_2O_2), AO/e-H_2O_2/UVC and AO/UVC, and the isolated AO and UVC processes were evaluated in order to elucidate the individual and synergistic contribution of each oxidative pathway in the degradation and mineralization of the aquatic

https://doi.org/10.1021/acs.iecr.6c00181
Ind. Eng. Chem. Res. XXXX, XXX, XXX−XXX

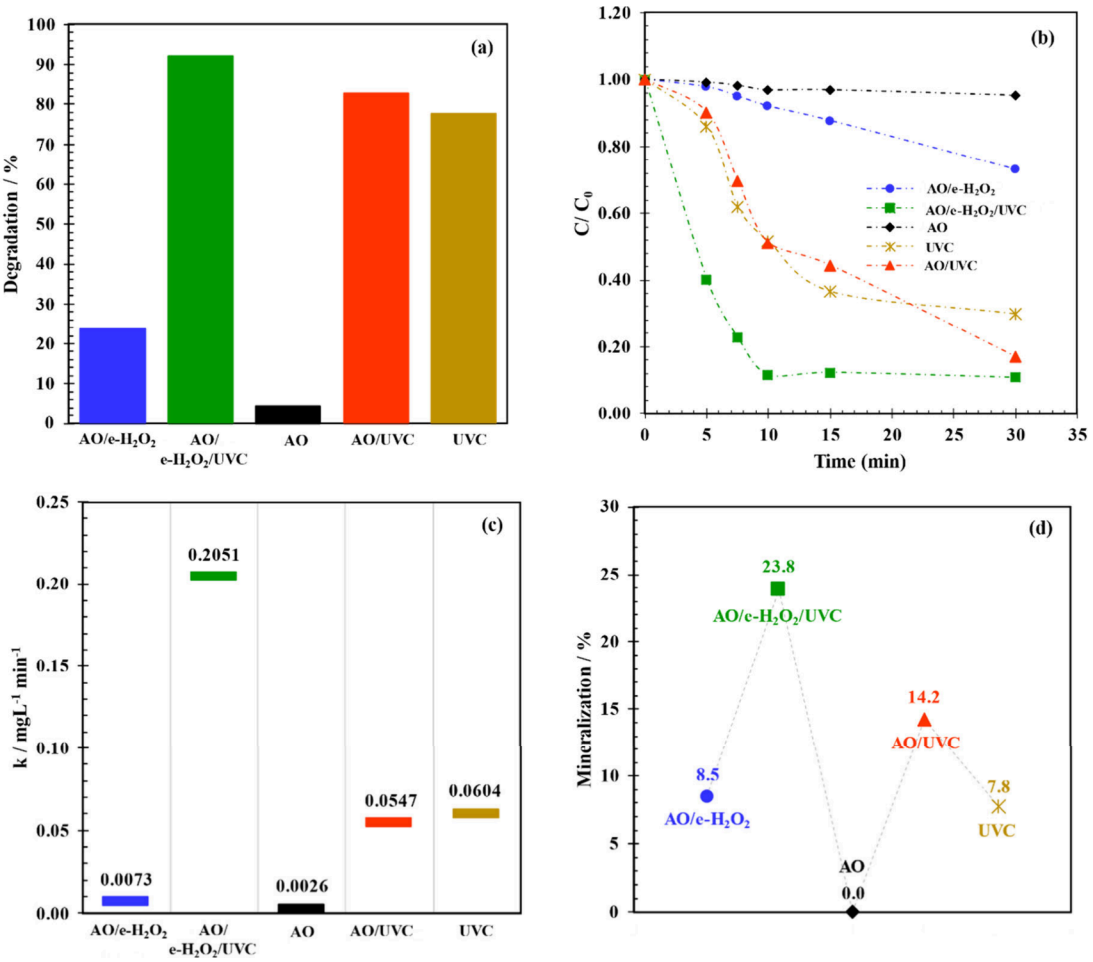

Figure 5. (a) Percentage of ATZ degradation (C_0 = 10 mg L^{-1}), (b) profiles of the different AOPs investigated (C/C_0), (c) apparent pseudo-first order kinetic constants (mg L^{-1} min^{-1}) and (d) mineralization rates for the different AOPs applied for AZT degradation in the concentric-cube electrochemical reactor. (Conditions: T = 20 °C, Qv = 400 mL min^{-1}, t = 30 min, K_2SO_4 = 0.075 mol L^{-1}, j = 20 mA cm^{-2}, and O_2 flow = 0.05 L min^{-1}, and pH 5.0.)

matrix. It should be noted that, in processes without H_2O_2 generation, N_2 was used under the optimized flow of O_2 to ensure comparable experimental conditions.

Although sulfate ions are commonly classified as inert in H_2O_2 electrogeneration, under the experimental conditions employed in this study, peroxomonosulfate (SO_5^{2-}) can form during electrolysis at low K_2SO_4 concentrations (eq 11). This species can subsequently react with H_2O_2 (eq 12), reducing its effective concentration in the system.[20,28,48] Therefore, while H_2O_2 is the primary oxidizing agent responsible for atrazine degradation, it is important to acknowledge that sulfate-derived species may also contribute to the overall oxidative process, potentially influencing the reaction kinetics and oxidant availability.

$$H_2O + SO_4^{2-} \rightarrow 2H^+ + SO_5^{2-} + 2e^- \quad (11)$$

$$H_2O_2 + SO_5^{2-} \rightarrow 2O_2 + H_2SO_4 \quad (12)$$

Figure 5a shows the degradation efficiencies obtained in each AOP. After 30 min of electrolysis, anodic oxidation alone exhibited the worst performance, recording roughly 5% ATZ degradation. The combined AO/UVC and AO/e-H_2O_2/UVC processes exhibited significantly superior performance, with ATZ removal rates of 82.9% and 92.3%, respectively. The isolated application of UVC also promoted efficient ATZ degradation, approximately 77.0%. On the other hand, the AO/e-H_2O_2 alone recorded only 24.0% ATZ degradation, demonstrating that the presence of only electrogenerated H_2O_2 was not sufficient to promote effective ATZ oxidation; this behavior can be attributed to the low activation efficiency of H_2O_2 in the absence of UVC radiation, since, without photolysis, the species remains mostly stable and acts more as a selective oxidant than as an efficient source of $^{\bullet}OH$.[49,50] Furthermore, the slow kinetics of the direct reaction between H_2O_2 and atrazine and the possibility of competitive recombination of the peroxide may contribute to the low observed efficiency. In contrast, in photoassisted oxidation systems, UVC irradiation can promote the decomposition of H_2O_2 into highly reactive $^{\bullet}OH$ species (E° = 2.80 V vs SHE),[28] as represented in eq 13,[49,50] which justifies the marked improvement in degradation observed under the combined oxidation processes.

$$H_2O_2 \xrightarrow{h\nu_{UVC}} 2HO^{\bullet} \quad (13)$$

Figure 5b shows the ATZ degradation profiles (C/C_0) recorded based on the application of the different AOPs investigated over time. This temporal analysis shows that the AO/e-H_2O_2/UVC process has a significant efficiency advantage over the other processes, especially in the first 10 min of

https://doi.org/10.1021/acs.iecr.6c00181
Ind. Eng. Chem. Res. XXXX, XXX, XXX−XXX

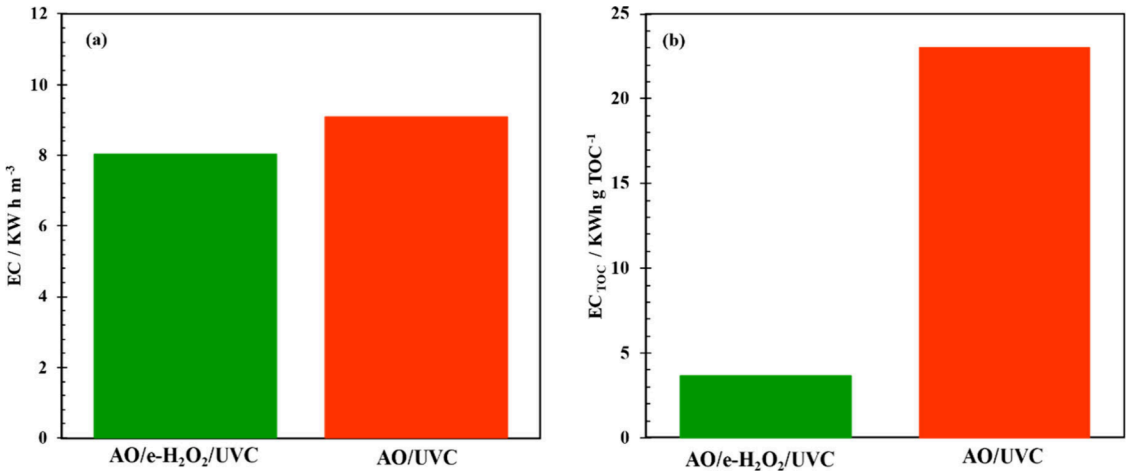

Figure 6. (a) Energy consumption per treated volume and (b) energy consumption normalized by the TOC mass removed and mineralization current efficiency obtained for the AO/e-H_2O_2/UVC and AO/UVC treatment processes applied for AZT degradation in the concentric-cube electrochemical reactor. (Conditions: T = 20 °C, Q_v = 400 mL min^{-1}, t = 30 min, K_2SO_4 = 0.075 mol L^{-1}, j = 20 mA cm^{-2}, O_2 flow = 0.05 L min^{-1} and pH = 5.0.)

electrolysis, when more than 90.0% of ATZ is degraded. In contrast, the AO/UVC and UVC-only processes exhibited more moderate degradation profiles, although superior to those of AO/e-H_2O_2 without irradiation, which confirms the importance of photochemical activation in intensifying the oxidation process. The poor performance recorded by AO-only, with almost no degradation over time, shows that the exclusive contribution of anodically generated oxidizing species is not sufficient for the rapid degradation of ATZ in solution. This degradation kinetics of atrazine still indicates that mass-transport limitations related to corners have a negligible effect on contaminant removal. The recirculation flow, along with the positioning of the reactor inlet and outlet, promotes uniform convective transport and continuous electrolyte renewal on the electrode surfaces, ensuring effective mixing throughout the reactor. These results reinforce that the reactor geometry does not significantly compromise the overall degradation performance.

Figure 5c shows the apparent pseudo-first-order kinetic constants (mg L^{-1} min^{-1}) for ATZ degradation in each AOP in the first 10 min. It can be observed that the AO/e-H_2O_2/UVC process exhibited the highest kinetic constant (0.2051 min^{-1}), confirming its high efficiency in AZT degradation. The UVC-only and AO/UVC processes recorded intermediate k values, 0.0604 min^{-1} and 0.0547 min^{-1}, respectively. Despite the fact that the degradation results recorded for the UVC-only and AO/UVC processes were quite close, as shown in Figure 5a, the result obtained from the combined process (AO/e-H_2O_2/UVC) was 1 order of magnitude higher than that of the UVC-only; in essence, this points to the advantage of using the combined approach to improve the degradation rate. In contrast, the AO/e-H_2O_2 and AO-only processes recorded very low k values, 0.0073 min^{-1} and 0.0026 min^{-1}, respectively, which is clearly consistent with the limited behavior observed for these processes in the temporal profiles in Figure 5b. These results highlight the influential role played by the photochemical activation of H_2O_2 in the kinetic intensification of the process, making AO/e-H_2O_2/UVC the most promising technique for the rapid degradation of ATZ.

Figure 5d shows the relative efficiency of the different treatment processes in terms of mineralization expressed by the comparative TOC index. Assessing mineralization is essentially crucial because it allows one to verify not only the partial degradation of the target molecule but also its conversion into less harmful inorganic species.[51] The combined AO/e-H_2O_2 process and the sole UVC process exhibited modest mineralization percentages, corresponding to 8.5% and 7.8%, respectively, while the sole AO process did not even promote any partial mineralization. In contrast, the AO/e-H_2O_2/UVC process recorded the highest mineralization percentage, 23.8%, clearly standing out from the other processes. The AO/UVC process recorded the second highest rate, slightly above 14%. These results demonstrate that the synergy between the combined processes assisted by UVC radiation is efficient not only for the degradation of atrazine but also for its mineralization; this shows that the use of combined treatment processes, such as AO/e-H_2O_2/UVC, in the presence of UVC represents the most promising strategy for accelerating the breakdown of the AZT molecule and overcoming the limitations inherent to each of the isolated treatment techniques.

3.6. Comparative Analysis of the Efficiency of the Degradation Process under Optimized Conditions in UVC-Assisted Processes

When it comes to analyzing the efficiency of combined UVC-assisted treatment processes, it is essential to evaluate not only the efficiency in terms of degradation and mineralization but also the associated energy parameters. The energy efficiency of the AOPs investigated in this study was assessed based on energy consumption per treated volume (EC), and energy consumption normalized by the mass of TOC removed. This analysis is crucial because it provides one with a thorough understanding regarding the practical feasibility of the processes, since their full-scale application depends directly on the relationship between removal efficiency and energy costs.[29]

As shown in Figure 6a, the AO/e-H_2O_2/UVC process recorded a specific energy consumption of 8.02 kWh m^{-3}, slightly lower than that observed for AO/UVC, which was 9.08 kWh m^{-3}. However, when normalized by the TOC removed (Figure 6b), a significant advantage is observed for the AO/e-H_2O_2/UVC process, which consumed only 3.63 kWh of

https://doi.org/10.1021/acs.iecr.6c00181
Ind. Eng. Chem. Res. XXXX, XXX, XXX−XXX

g_{TOC}^{-1} in contrast to the 23.04 kWh of g_{TOC}^{-1} consumed under the AO/UVC process. This advantage is attributed to the continuous electrogeneration of H_2O_2 in the AO/e-H_2O_2/UVC process, which ensures its greater availability for the formation of photoactivated $^{\bullet}OH$ and promotes more efficient mineralization. The balance between degradation efficiency, mineralization, and energy costs shows that the AO/e-H_2O_2/UVC process represents the most advantageous alternative to traditional treatment processes and has been proven to be the most promising route for AZT degradation.

3.7. LC−MS/MS Analysis of the Pathways Involving the Oxidation of ATZ and Its Intermediates

The pathways involving the degradation of AZT and its intermediates in the AO/e-H_2O_2/UVC process were elucidated through the application of electrospray mass spectrometry (ESI/MS) analyses. The spectra of the initial aliquot, prior to the AO/e-H_2O_2/UVC treatment, confirmed the presence of ATZ, with a protonated ion peak $[M + H]^+$ at m/z 216.10. Based on the proposed structures of the 11 resulting products (Table 4), the possible pathway for AZT degradation was inferred, which primarily involved the reaction channels illustrated in Figure 7. The degradation routes observed in this study are consistent with those reported for other ATZ degradation processes which are based on oxidative systems.[52−57] The Supporting Information contains the LC−MS/MS chromatograms of the identified fragments of AZT intermediates (Figures S2−S13).

Table 4. Identification of ATZ Degradation Intermediates by LC−MS/MS Analysis, Including Their Proposed Structures and Corresponding m/z Values

Product	RT (min)	Molecular Ion (m/z)	Molecular formula
ATZ 1	3.01	198.14	$C_8H_{15}N_5O$
ATZ 2	2.36	212.11	$C_8H_{13}N_5O_2$
ATZ 3	7.30	284.03	$C_8H_5N_5O_7$
ATZ 4	7.22	271.09	$C_6H_{14}N_4O_8$
ATZ 5	7.01	279.09	$C_8H_{14}N_4O_7$
ATZ 6	0.97	311.08	$C_8H_{14}N_4O_9$
ATZ 7	6.76	304.01	$C_8H_6ClN_5O_6$
ATZ 8	4.80	188.07	$C_6H_{10}ClN_5$
ATZ 9	5.41	252.05	$C_6H_{10}ClN_5O_4$
ATZ 10	11.02	352.12	$C_8H_{22}ClN_5O_8$
ATZ 11	8.90	383.08	$C_8H_{19}ClN_4O_{11}$

One pathway of AZT degradation involved the substitution of the chlorine atom by a hydroxyl group (dechlorination) on the s-triazine ring, which gave rise to hydroxyatrazine (ATZ 1, m/z 198.14).[53−55] A further attack on hydroxyatrazine by hydroxyl radicals led to the formation of oxidized or hydroxylated intermediates. The attack of the radicals was initially targeted at the ethanamine side chain, which resulted in the formation of ATZ 2 (m/z 212.11).[52,57] A subsequent oxidation of the ATZ 2 side chains promoted the conversion of the methyl group ($-CH_3$) into an aldehyde ($-CHO$), followed by further oxidation to a carboxylic acid ($-COOH$), which generated the carboxylated derivative ATZ 3 (m/z 284.03).[53] Oxidative carboxylation associated with s-triazine ring cleavage gave rise to derivative ATZ 4 (m/z 271.09). Similarly, carboxylation of the hydroxyatrazine side chains coupled with ring opening led to the formation of ATZ 5 (m/z = 279.09), which was further hydroxylated in the ethanamine group to produce ATZ 6 (m/z = 311.08).

Sequential oxidation of atrazine was also observed independently of dechlorination, which yielded carbonyl product ATZ 7 (m/z 304.01). With deeper oxidation, the s-triazine ring underwent successive hydroxylation, substitution, and hydrolysis reactions, generating highly oxygenated derivatives including ATZ 10 (m/z 352.12) and ATZ 11 (m/z 383.08).[56] Another pathway for the degradation of AZT and its intermediates involved N-dealkylation (desethylation). Radicals attacked the alkyl chains attached to nitrogen, and this led to the formation of desethylatrazine (ATZ 8, m/z 188.07) and its hydroxylated derivative ATZ 9 (m/z 252.05).[52,53,55]

4. CONCLUSIONS

The results obtained from this work demonstrated that the continuous-flow electrochemical reactor, developed using a concentric-cube geometry, is an efficient and sustainable system for the in-situ generation of H_2O_2 and advanced

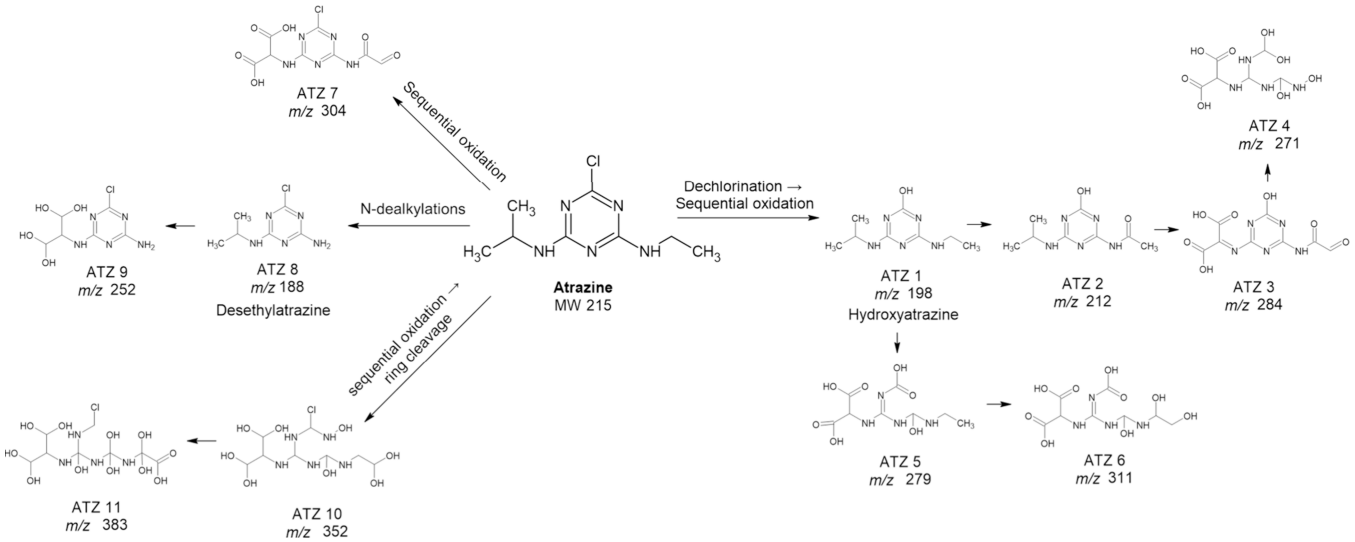

Figure 7. Proposed pathways for ATZ degradation under the AO/e-H_2O_2/UVC treatment process showing the main intermediates identified via LC−MS/MS analysis.

https://doi.org/10.1021/acs.iecr.6c00181
Ind. Eng. Chem. Res. XXXX, XXX, XXX−XXX

water treatment applications. The CCRD optimization analysis (The CCRD optimization (x_1 - K_2SO_4 = 0.075 mol L^{-1}, x_2 − j = 20 mA cm^{-2}, x_3 − O_2 flow of 0.05 L min^{-1}, and x_4 − pH = 5.0) revealed that current density and pH are the most critical parameters for maximizing current efficiency and minimizing energy consumption. Under these conditions, the production/accumulation of H_2O_2 was the second highest during the delineation, reaching 848.8 mg L^{-1} of H_2O_2.

The mathematical model developed through CCRD successfully explained more than 96% of the experimental variability, while ANOVA results confirmed that the model was statistically significant and predictive ($p < 0.05$). Under the optimized conditions, the reactor produced high H_2O_2 concentrations with excellent stability and good energy efficiency. When applied toward ATZ degradation, the combined AO/e-H_2O_2/UVC process exhibited strong synergistic effects, recording over 90.0% AZT degradation and partial mineralization in 30 min of electrolysis. LC−MS/MS analysis identified 11 oxidative intermediates and helped elucidate the pathways involving AZT degradation, confirming the effective transformation of ATZ through dechlorination, hydroxylation, and cleavage of the s-triazine ring.

Importantly, the geometric characteristics of the reactor were found to be critical for its performance. Key factors include the spatial arrangement of the electrodes to maximize reactive surface area, the distance between the anode and cathode to optimize mass transport and minimize ohmic losses, and the configuration of the gas and liquid compartments to ensure efficient oxygen diffusion and uniform electrolyte distribution. Careful design of these parameters is essential to achieve high H_2O_2 electrogeneration efficiency and effective contaminant degradation, providing valuable guidance for the scaleup and implementation of similar electrochemical treatment systems.

Overall, the study highlights the technological potential of this innovative reactor configuration to promote efficient H_2O_2 electrogeneration and the remediation of persistent contaminants, reinforcing its relevance and suitability for application in sustainable electrochemical water treatment systems.

■ ASSOCIATED CONTENT

Supporting Information

The Supporting Information is available free of charge at https://pubs.acs.org/doi/10.1021/acs.iecr.6c00181.

Characterization of GDE/PL6C and LC-MS fragments of intermediate of atrazine (PDF)

(PDF)

■ AUTHOR INFORMATION

Corresponding Authors

Raul José Alves Felisardo − *São Carlos Institute of Chemistry, University of São Paulo, São Carlos, SP 13566-590, Brazil;* orcid.org/0000-0003-3686-214X; Email: rfelisardo@usp.br

Robson da Silva Souto − *São Carlos Institute of Chemistry, University of São Paulo, São Carlos, SP 13566-590, Brazil;* orcid.org/0000-0001-9142-0665; Email: robsonssouto@gmail.com

Marcos Roberto de Vasconcelos Lanza − *São Carlos Institute of Chemistry, University of São Paulo, São Carlos, SP 13566-590, Brazil*; Email: marcoslanza@usp.br

Authors

Andre Luis Carvalho Souza − *São Carlos Institute of Chemistry, University of São Paulo, São Carlos, SP 13566-590, Brazil*

Renata Colombo − *School of Arts, Sciences and Humanities, University of São Paulo, São Paulo, SP 03828-000, Brazil*

Complete contact information is available at: https://pubs.acs.org/10.1021/acs.iecr.6c00181

Author Contributions

All authors contributed to the study conception and design. **Andre Luis Carvalho Souza**: Conceptualization, methodology, investigation, validation, formal analysis, visualization, data curation, writing − original draft, writing − review and editing. **Raul José Alves Felisardo**: Investigation, validation, formal analysis, writing − original draft, writing − review and editing. **Robson da Silva Souto**: Investigation, validation, formal analysis, writing − original draft, writing − review and editing. **Renata Colombo**: Methodology, formal analysis, writing − original draft, writing - review and editing. **Marcos Roberto de Vasconcelos Lanza**: Conceptualization, supervision, project administration, funding acquisition, writing − review and editing. All authors read and granted their approval of the final manuscript.

Funding

The Article Processing Charge for the publication of this research was funded by the Coordenacao de Aperfeicoamento de Pessoal de Nivel Superior (CAPES), Brazil (ROR identifier: 00x0ma614).

Notes

The authors declare no competing financial interest.

■ ACKNOWLEDGMENTS

This study was partially funded by the São Paulo Research Foundation (FAPESP), Brazil, (Process Nos. #2023/16462-5, #2023/13260-2, #2024/20854-9, #2018/22210-0, #2018/22211-7, #2018/22022-0, #2019/06650-3 and #2022/12895-1) and the Brazilian National Council for Scientific and Technological Development − CNPq (Grant #303943/2021-1 and 401122/2025-5).

■ REFERENCES

(1) Kariyanna, B.; Senthil-Nathan, S.; Vasantha-Srinivasan, P.; Subba Reddy, B. V.; Krishnaiah, A.; Meenakshi, N. H.; Han, Y. S.; Karthi, S.; Chakravarthy, A. K.; Park, K. B. Comprehensive Insights into Pesticide Residue Dynamics: Unraveling Impact and Management. *Chem. Biol. Technol. Agric.* **2024**, *11* (1), 182.

(2) Rosa Barbosa, M. P.; Lima, N. S.; de Matos, D. B.; Alves Felisardo, R. J.; Santos, G. N.; Salazar-Banda, G. R.; Cavalcanti, E. B. Degradation of Pesticide Mixture by Electro-Fenton in Filter-Press Reactor. *J. Water Process Eng.* **2018**, *25*, 222−235.

(3) Bhatia, T.; Sindhu, S. S. Sustainable Management of Organic Agricultural Wastes: Contributions in Nutrients Availability, Pollution Mitigation and Crop Production. *Discover Agric.* **2024**, *2* (1), 130.

(4) Brillas, E.; Martínez-Huitle, C. A. Decontamination of Wastewaters Containing Synthetic Organic Dyes by Electrochemical Methods. An Updated Review. *Appl. Catal., B* **2015**, *166−167*, 603−643.

(5) Barbieri, M. V.; Monllor-Alcaraz, L. S.; Postigo, C.; López de Alda, M. Improved Fully Automated Method for the Determination of Medium to Highly Polar Pesticides in Surface and Groundwater and Application in Two Distinct Agriculture-Impacted Areas. *Sci. Total Environ.* **2020**, *745*, 140650.

(6) Li, Y.-F.; Hao, S.; Ma, W.-L.; Yang, P.-F.; Li, W.-L.; Zhang, Z.-F.; Liu, L.-Y.; Macdonald, R. W. Persistent Organic Pollutants in Global Surface Soils: Distributions and Fractionations. *Environ. Sci. Ecotechnol.* **2024**, *18*, 100311.
(7) Tao, Q.-H.; Tang, H.-X. Effect of Dye Compounds on the Adsorption of Atrazine by Natural Sediment. *Chemosphere* **2004**, *56* (1), 31−38.
(8) He, H.; Liu, Y.; You, S.; Liu, J.; Xiao, H.; Tu, Z. A Review on Recent Treatment Technology for Herbicide Atrazine in Contaminated Environment. *Int. J. Environ. Res. Public Health* **2019**, *16* (24), 5129.
(9) De Rosa, E.; Montuori, P.; Di Duca, F.; De Simone, B.; Scippa, S.; Nubi, R.; Provvisiero, D. P.; Russo, I.; Triassi, M. Assessment of Atrazine Contamination in the Sele River Estuary: Spatial Distribution, Human Health Risks, and Ecological Implications in Southern Europe. *Environ. Sci. Eur.* **2024**, *36* (1), 115.
(10) Hayes, T. B.; Khoury, V.; Narayan, A.; Nazir, M.; Park, A.; Brown, T.; Adame, L.; Chan, E.; Buchholz, D.; Stueve, T.; Gallipeau, S. Atrazine Induces Complete Feminization and Chemical Castration in Male African Clawed Frogs (*Xenopus Laevis*). *Proc. Natl. Acad. Sci. U. S. A.* **2010**, *107* (10), 4612−4617.
(11) Garcia-Segura, S.; Brillas, E. Applied Photoelectrocatalysis on the Degradation of Organic Pollutants in Wastewaters. *J. Photochem. Photobiol. C: Photochem. Rev.* **2017**, *31*, 1−35.
(12) Brillas, E.; Garcia-Segura, S. Recent Progress of Applied TiO2 Photoelectrocatalysis for the Degradation of Organic Pollutants in Wastewaters. *J. Environ. Chem. Eng.* **2023**, *11* (3), 109635.
(13) Martínez-Huitle, C. A.; Rodrigo, M. A.; Sirés, I.; Scialdone, O. Single and Coupled Electrochemical Processes and Reactors for the Abatement of Organic Water Pollutants: A Critical Review. *Chem. Rev.* **2015**, *115* (24), 13362−13407.
(14) Garcia-Segura, S.; Brillas, E. Applied Photoelectrocatalysis on the Degradation of Organic Pollutants in Wastewaters. *J. Photochem. Photobiol. C: Photochemistry Rev.* **2017**, *31*, 1−35.
(15) Olvera-Vargas, H.; Pazos, M.; Bustos, E.; Deng, F.; Salazar-González, R.; Oturan, M. A. Recent Developments in (Photo)-Electrocatalytic Materials for Wastewater Treatment and Resource Recovery. *Appl. Catal. O: Open* **2025**, *202*, 207033.
(16) Cordeiro-Junior, P. J. M.; Lobato Bajo, J.; Lanza, M. R. de V.; Rodrigo Rodrigo, M. A. Highly Efficient Electrochemical Production of Hydrogen Peroxide Using the GDE Technology. *Ind. Eng. Chem. Res.* **2022**, *61* (30), 10660−10669.
(17) Petsi, P.; Plakas, K.; Frontistis, Z.; Sirés, I. A Critical Assessment of the Effect of Carbon-Based Cathode Properties on the in Situ Electrogeneration of H2O2. *Electrochim. Acta* **2023**, *470*, 143337.
(18) Bimbi Júnior, F. E.; Junior, O. C.; Souto, R. S.; Encide, J. P. P.; Baruch, M. M.; Felipe, M. C. V.; Fernandes, L.; Araujo, I. F.; Fernandes, C. H. M.; Oliveira, I. G. S.; Honorio, K. M.; Colombo, R.; Mastelaro, V. R.; Barros, W. R. P.; Lanza, M. R. V. In-Situ Electrogeneration of H2O2 and Hydroxyl Radical Applied for Venlafaxine Degradation: A Novel Strategy Using FeSe2-Modified Carbon Gas Diffusion Electrode. *Chem. Eng. J.* **2025**, *517*, 164432.
(19) Oliveira Silva, T.; Granados-Fernández, R.; Lobato, J.; Lanza, M. R. V.; Rodrigo, M. A. Boosting New Electrochemical Reactor Designs to Improve the Performance in H_2O_2 Production Using Gas Diffusion Electrodes. *ACS Sustain. Chem. Eng.* **2025**, *13* (8), 3172−3182.
(20) Marques Cordeiro-Junior, P. J.; Sáez Jiménez, C.; Vasconcelos Lanza, M. R. de; Rodrigo Rodrigo, M. A. Electrochemical Production of Extremely High Concentrations of Hydrogen Peroxide in Discontinuous Processes. *Sep. Purif. Technol.* **2022**, *300*, 121847.
(21) Alves Felisardo, R. J.; Magalhães Fernandes, C. H.; de Oliveira Santiago Santos, G.; de Vasconcelos Lanza, M. R. Unlocking the Potential of in Situ H2O2 Generation in Urine as a Decentralized Electro-Sanitation Strategy. *Chem. Eng. J.* **2025**, *507*, 160391.
(22) Fernandes, C. H. M.; E-Durán, F.; Santos, G. O. S.; Felisardo, R. J. A.; Colombo, R.; Barros, W. R. P.; Lanza, M. R. V. Exploring the Potential of H2O2 Electrogenerated through Gas Diffusion Electrode to Enhance Caffeine Degradation in Real-World Water Matrices. *Sep. Purif. Technol.* **2026**, *381*, 135487.
(23) Magdaleno, A. L.; Cerrón-Calle, G. A.; dos Santos, A. J.; Lanza, M. R. V.; Apul, O. G.; Garcia-Segura, S. Unlocking the Potential of Nanobubbles: Achieving Exceptional Gas Efficiency in Electrogeneration of Hydrogen Peroxide. *Small* **2024**, *20* (3), DOI: 10.1002/smll.202304547.
(24) Silva, T. O.; Goulart, L. A.; Sánchez-Montes, I.; Santos, G. O. S.; Santos, R. B.; Colombo, R.; Lanza, M. R. V. Using a Novel Gas Diffusion Electrode Based on PL6 Carbon Modified with Benzophenone for Efficient H2O2 Electrogeneration and Degradation of Ciprofloxacin. *Chem. Eng. J.* **2023**, *455*, 140697.
(25) Li, Y.; Zhang, Y.; Xia, G.; Zhan, J.; Yu, G.; Wang, Y. Evaluation of the Technoeconomic Feasibility of Electrochemical Hydrogen Peroxide Production for Decentralized Water Treatment. *Front. Environ. Sci. Eng.* **2021**, *15* (1), 1.
(26) Muddemann, T.; Haupt, D.; Sievers, M.; Kunz, U. Elektrochemische Reaktoren Für Die Wasserbehandlung. *Chemie Ingenieur Technik* **2019**, *91* (6), 769−785.
(27) Valim, R. B.; Reis, R. M.; Castro, P. S.; Lima, A. S.; Rocha, R. S.; Bertotti, M.; Lanza, M. R. V. Electrogeneration of Hydrogen Peroxide in Gas Diffusion Electrodes Modified with Tert-Butyl-Anthraquinone on Carbon Black Support. *Carbon N. Y.* **2013**, *61*, 236−244.
(28) Escalona-Durán, F.; Fernandes, C. H. M.; Doria, A. R.; Santos, G. O. S.; Colombo, R.; Barros, W. R. P.; Lanza, M. R. V. Evaluating the Synergistic Effect of UVC/e-H2O2 Applied for Benzotriazole Degradation in Water Matrices Using Catalyst-Free Printex L6 Carbon-Based Gas Diffusion Electrode. *Chemosphere* **2025**, *370*, 144016.
(29) Felisardo, R. J. A.; dos Santos, G. N.; Leite, M. S.; Ferreira, L. F. R.; Garcia-Segura, S.; Cavalcanti, E. B. Decentralized Electro-Sanitation System as Proof of Concept to Treat Urine Produced in Long-Distance Bus. *Process Safety Environ. Protect.* **2024**, *182*, 20.
(30) Stirling, R.; Walker, W. S.; Westerhoff, P.; Garcia-Segura, S. Techno-Economic Analysis to Identify Key Innovations Required for Electrochemical Oxidation as Point-of-Use Treatment Systems. *Electrochim. Acta* **2020**, *338*, 135874.
(31) Rodrigues, M. I.; Iemma, A. F. *Experimental Design and Process Optimization*; CRC Press, 2014, DOI: 10.1201/b17848.
(32) Huang, Y.; Fan, H.; Yip, N. Y. Influence of Electrolyte on Concentration-Induced Conductivity-Permselectivity Tradeoff of Ion-Exchange Membranes. *J. Membr. Sci.* **2023**, *668*, 121184.
(33) Han, J.; Bai, X.; Xu, X.; Bai, X.; Husile, A.; Zhang, S.; Qi, L.; Guan, J. Advances and Challenges in the Electrochemical Reduction of Carbon Dioxide. *Chem. Sci.* **2024**, *15* (21), 7870−7907.
(34) da Silva Souto, R.; Souza, L. P. de; Cordeiro Junior, P. J. M.; Ramos, B.; Teixeira, A. C. S. C.; Rocha, R. da S.; Lanza, M. R. V. Insights into Hydrodynamic and Operational Conditions for Scalable Hydrogen Peroxide Electrosynthesis Applications. *Ind. Eng. Chem. Res.* **2023**, *62* (37), 15084−15097.
(35) Mattos, I. L. de; Shiraishi, K. A.; Braz, A. D.; Fernandes, J. R. Peróxido de Hidrogênio: Importância e Determinação. *Quim. Nova* **2003**, *26* (3), 373−380.
(36) Chai, X.-S.; Hou, Q. X.; Luo, Q.; Zhu, J. Y. Rapid Determination of Hydrogen Peroxide in the Wood Pulp Bleaching Streams by a Dual-Wavelength Spectroscopic Method. *Anal. Chim. Acta* **2004**, *507* (2), 281−284.
(37) Zhou, W.; Meng, X.; Gao, J.; Alshawabkeh, A. N. Hydrogen Peroxide Generation from O2 Electroreduction for Environmental Remediation: A State-of-the-Art Review. *Chemosphere* **2019**, *225*, 588−607.
(38) Zhou, W.; Meng, X.; Gao, J.; Alshawabkeh, A. N. Hydrogen Peroxide Generation from O2 Electroreduction for Environmental Remediation: A State-of-the-Art Review. *Chemosphere* **2019**, *225*, 588−607.
(39) Sun, Y.; Fan, K.; Li, J.; Wang, L.; Yang, Y.; Li, Z.; Shao, M.; Duan, X. Boosting Electrochemical Oxygen Reduction to Hydrogen

https://doi.org/10.1021/acs.iecr.6c00181
Ind. Eng. Chem. Res. XXXX, XXX, XXX−XXX

Peroxide Coupled with Organic Oxidation. *Nat. Commun.* **2024**, *15* (1), 6098.
(40) Daghrir, R.; Drogui, P.; Robert, D. Photoelectrocatalytic Technologies for Environmental Applications. *J. Photochem. Photobiol. A Chem.* **2012**, *238*, 41−52.
(41) Ragnini, C. A. R.; Di Iglia, R. A.; Bertazzoli, R. Considerações Sobre a Eletrogeração de Peróxido de Hidrogênio. *Quim. Nova* **2001**, *24* (2), 252−256.
(42) Zhang, Q.; Zheng, L.; Gu, F.; Wu, J.; Gao, J.; Zhang, Y.-C.; Zhu, X.-D. Recent Advances in Single-Atom Catalysts for Acidic Electrochemical Oxygen Reduction to Hydrogen Peroxide. *Nano Energy* **2023**, *116*, 108798.
(43) Qiang, Z.; Chang, J.-H.; Huang, C.-P. Electrochemical Generation of Hydrogen Peroxide from Dissolved Oxygen in Acidic Solutions. *Water Res.* **2002**, *36* (1), 85−94.
(44) Sibiya, N. P.; Amo-Duodu, G.; Kweinor Tetteh, E.; Rathilal, S. Response Surface Optimisation of a Magnetic Coagulation Process for Wastewater Treatment via Box-Behnken. *Mater. Today Proc.* **2022**, *62*, S122−S126.
(45) dos Santos, G. N.; Felisardo, R. J. A.; Chagas, T. S. A.; dos Santos Freitas, L.; Eguiluz, K. I. B.; Cavalcanti, E. B. Electrochemical Treatment of Agro-Industrial Effluent: Integrating Response Surface Methodology and Neural Networks for Sustainable Solutions. *J. Water Process Eng.* **2025**, *73*, 107743.
(46) Rodrigues, M. I.; Iemma, A. F. *Experimental Design and Process Optimization*, 1st Edition; CRC Press, 2014.
(47) Altland, H. W. Regression Analysis: Statistical Modeling of a Response Variable. *Technometrics* **1999**, *41* (4), 367−368.
(48) Felisardo, R. J. A.; Durán, F. E.; Fernandes, C. H. M.; de Oliveira Santiago Santos, G.; Colombo, R.; Rodrigo, M. A. R.; de Vasconcelos Lanza, M. R. Enhanced H2O2 Electrogeneration for Simultaneous Degradation of Multiple Pharmaceuticals and Validation in Real Water Using UVC-Assisted Processes. *Chem. Eng. J.* **2026**, *529*, 172801.
(49) Brillas, E. A Review on the Photoelectro-Fenton Process as Efficient Electrochemical Advanced Oxidation for Wastewater Remediation. Treatment with UV Light, Sunlight, and Coupling with Conventional and Other Photo-Assisted Advanced Technologies. *Chemosphere* **2020**, *250*, 126198.
(50) Barazorda-Ccahuana, H. L.; Fajardo, A. S.; dos Santos, A. J.; Lanza, M. R. V. Decentralized Approach toward Organic Pollutants Removal Using UV Radiation in Combination with H2O2-Based Electrochemical Water Technologies. *Chemosphere* **2023**, *342*, 140079.
(51) Felisardo, R. J. A.; Brillas, E.; Boyer, T. H.; Cavalcanti, E. B.; Garcia-Segura, S. Electrochemical Degradation of Acetaminophen in Urine Matrices: Unraveling Complexity and Implications for Realistic Treatment Strategies. *Water Res.* **2024**, *261*, 122034.
(52) Zhang, J.; Zhuang, T.; Liu, S.; Sun, S.; Wang, Y.; Liu, X.; Wang, J.; Liu, R. Catalytic Ozonation of Atrazine Enhanced by Mesoporous CeO2: Morphology, Performance and Intermediates. *Water (Basel).* **2022**, *14* (21), 3431.
(53) Gao, J.; Zhao, X.; Li, C.; Luo, Z.; Zhang, L.; Xiao, Z.; Mu, T.; Liu, F.; Gao, R.; Zhang, J.; Sun, X. Efficient Atrazine Degradation through ZnFe2O4-Catalyzed Peroxymonosulphate Activation. *Sci. Rep.* **2025**, *15* (1), 15184.
(54) Mu, Y.; Zhan, G.; Huang, C.; Wang, X.; Ai, Z.; Zou, J.; Luo, S.; Zhang, L. Dechlorination-Hydroxylation of Atrazine to Hydroxyatrazine with Thiosulfate: A Detoxification Strategy in Seconds. *Environ. Sci. Technol.* **2019**, *53* (6), 3208−3216.
(55) Zhang, J. J.; Lu, Y. C.; Yang, H. Chemical Modification and Degradation of Atrazine in *Medicago Sativa* through Multiple Pathways. *J. Agric. Food Chem.* **2014**, *62* (40), 9657−9668.
(56) Tauber, A.; von Sonntag, C. Products and Kinetics of the OH-Radical-Induced Dealkylation of Atrazine. *Acta Hydrochim. Hydrobiol.* **2000**, *28* (1), 15−23.
(57) Zajíček, P.; Kolář, M.; Prucek, R.; Ranc, V.; Bednář, P.; Varma, R. S.; Sharma, V. K.; Zbořil, R. Oxidative Degradation of Triazine- and Sulfonylurea-Based Herbicides Using Fe(VI): The Case Study of Atrazine and Iodosulfuron with Kinetics and Degradation Products. *Sep. Purif. Technol.* **2015**, *156*, 1041−1046.

https://doi.org/10.1021/acs.iecr.6c00181
Ind. Eng. Chem. Res. XXXX, XXX, XXX−XXX